

# Neutrino Oscillation Effects on Supernova Light Element Synthesis

Takashi Yoshida<sup>1,2</sup>, Toshitaka Kajino<sup>3,4</sup>, Hidekazu Yokomakura<sup>5</sup>, Keiichi Kimura<sup>5</sup>,  
Akira Takamura<sup>6</sup>, Dieter H. Hartmann<sup>7</sup>

<sup>1</sup>*Astronomical Institute, Graduate School of Science, Tohoku University, Aramaki,  
Aoba-ku, Sendai, Miyagi 980-8578, Japan*

<sup>2</sup>*National Astronomical Observatory of Japan, 2-21-1 Osawa, Mitaka, Tokyo 181-8588,  
Japan*

takashi.yoshida@nao.ac.jp

<sup>3</sup>*National Astronomical Observatory of Japan, and The Graduate University for Advanced  
Studies, 2-21-1 Osawa, Mitaka, Tokyo 181-8588, Japan*

<sup>4</sup>*Department of Astronomy, Graduate School of Science, University of Tokyo, 7-3-1 Hongo,  
Bunkyo-ku, Tokyo 113-0033, Japan*

<sup>5</sup>*Department of Physics, Graduate School of Science, Nagoya University, Furo-cho,  
Chikusa-ku, Nagoya, Aichi 464-8602, Japan*

<sup>6</sup>*Department of Mathematics, Toyota National College of Technology, Eisei-cho 2-1,  
Toyota, Aichi 471-8525, Japan*

<sup>7</sup>*Department of Physics and Astronomy, Clemson University, Clemson, SC 29634, USA*

## ABSTRACT

Neutrino oscillations affect light element synthesis through the  $\nu$ -process in supernova explosions. The  ${}^7\text{Li}$  and  ${}^{11}\text{B}$  yields produced in a supernova explosion of a  $16.2 M_{\odot}$  star model increase by factors of 1.9 and 1.3 in the case of large mixing angle solution with normal mass hierarchy and  $\sin^2 2\theta_{13} \gtrsim 2 \times 10^{-3}$  compared with those without the oscillations. In the case of inverted mass hierarchy or nonadiabatic 13-mixing resonance, the increment of their yields is much smaller. Neutrino oscillations raise the reaction rates of charged-current  $\nu$ -process reactions in the region outside oxygen-rich layers. The number ratio of  ${}^7\text{Li}/{}^{11}\text{B}$  could be a tracer of normal mass hierarchy and relatively large  $\theta_{13}$ , still satisfying  $\sin^2 2\theta_{13} \leq 0.1$ , through future precise observations in stars having strong supernova component.

*Subject headings:* neutrinos — nuclear reactions, nucleosynthesis, abundances —  
supernovae: general

## 1. Introduction

In the final evolutionary stage of massive stars, most region of the stars except collapsing core explodes as supernova explosions. The collapsing core releases its gravitational energy with gigantic amount of neutrinos. The emitted neutrinos interact with nuclei in the exploding material and new species of nuclei are produced; this synthetic process is called the  $\nu$ -process (Domogatsky, Eramzhyan, & Nadyozhin 1978; Woosley et al. 1990). There are several species produced through the  $\nu$ -process. For light elements,  ${}^7\text{Li}$  and  ${}^{11}\text{B}$  are mainly produced through the  $\nu$ -process (Woosley et al. 1990; Woosley & Weaver 1995; Yoshida, Emori, & Nakazawa 2000; Rauscher et al. 2002; Yoshida et al. 2004; Yoshida, Kajino, & Hartmann 2005). Some  ${}^{19}\text{F}$  is also produced through the  $\nu$ -process (Woosley et al. 1990; Woosley & Weaver 1995; Rauscher et al. 2002). For neutron-deficient heavy nuclei  ${}^{138}\text{La}$  and  ${}^{180}\text{Ta}$  are also produced through charged-current interactions with  $\nu_e$  (Goriely et al. 2001; Heger et al. 2005). Neutrino-driven winds from proto-neutron stars are considered to be one of the promoting sites for  $r$ -process heavy elements (e.g., Woosley et al. 1994; Takahashi, Wittl, & Janka 1994; Otsuki et al. 2000; Terasawa et al. 2004).

Supernova explosion is one of the important sites for supplying  ${}^7\text{Li}$  and  ${}^{11}\text{B}$  as well as Galactic cosmic rays, AGB stars, and novae during Galactic chemical evolution (GCE) (e.g., Fields et al. 2000). In previous studies, we showed that the amounts of  ${}^7\text{Li}$  and  ${}^{11}\text{B}$  strongly depend on the neutrino energy spectra and the total neutrino energy (Yoshida et al. 2004, 2005). We also constrained the neutrino energy spectra from the gravitational energy of a proto-neutron star and GCE models (Yoshida et al. 2005). In these studies it has been assumed that the neutrino spectra do not change in the supernova ejecta.

On the other hand, recent remarkable progress in neutrino experiments has confirmed the phenomenon of neutrino oscillations (e.g., McKeown & Vogel 2004). The experiments on atmospheric neutrinos (e.g., Ashie et al. 2004), solar neutrinos (e.g., Ahmed et al. 2004), and reactor neutrinos (e.g., Apollonio et al. 2003; Araki et al. 2005) constrained most of parameter values in neutrino oscillations, such as squared mass differences and the mixing angles. Resultantly, the large mixing angle (LMA) solution turns out to be a unique solution for the 12- and 23-mixings. However, mass hierarchy between 1 and 3 mass eigenstates has not been clarified (e.g., Ashie et al. 2004) and only upper limit of  $\sin^2 2\theta_{13}$  has been determined (Apollonio et al. 2003).

Supernova neutrino is another promoting target for neutrino experiments. When SN 1987A occurred, Kamiokande group and IMB group found eleven and eight events of neutrino detection (Hirata et al. 1987; Bionta et al. 1987). Owing to the development of neutrino experiments, much larger events of the neutrino detection are expected when a supernova explosion occurs in neighboring galaxies. In order to evaluate the neutrino flux and their energy dependence, neutrino oscillations in supernova explosions have been investigated qualitatively (Dighe & Smirnov 2000) and quantitatively (Takahashi et al. 2001). They showed that in the case of adiabatic resonance for  $\sin^2 2\theta_{13}$  (LMA-L in Takahashi et al. 2001) the transition probability from  $\nu_e$  to  $\nu_{\mu,\tau}$  changes from 0 to almost 1 in the O/C layer in their supernova model. Finally, the energy spectrum of  $\nu_e$  changes to the one close to the  $\nu_{\mu,\tau}$  spectrum emitted from neutrino sphere. In the case of nonadiabatic resonance for  $\sin^2 2\theta_{13}$  (LMA-S in Takahashi et al. 2001), the change of neutrino spectra is smaller. The effects from mass hierarchy and from the change of the density profile due to the shock propagation were also investigated (Takahashi & Sato 2003; Takahashi et al. 2003).

Since neutrino oscillations change neutrino spectra, it is expected that the amounts of  ${}^7\text{Li}$  and  ${}^{11}\text{B}$  change by the effect of neutrino oscillations (Yoshida et al. 2006). During supernova explosions, neutral-current reactions such as  ${}^4\text{He}(\nu, \nu'p){}^3\text{H}$  and  ${}^4\text{He}(\nu, \nu'n){}^3\text{He}$  are important for  ${}^7\text{Li}$  and  ${}^{11}\text{B}$  production (Yoshida et al. 2004). We note here that the total reaction rates of neutral-current reactions do not change by the neutrino oscillations. The energy spectrum summed up in all neutrinos and antineutrinos does not change by the oscillations. On the other hand, the reaction rates of charged-current reactions such as  ${}^4\text{He}(\nu_e, e^-p){}^3\text{He}$  and  ${}^4\text{He}(\bar{\nu}_e, e^+n){}^3\text{H}$  are expected to increase by neutrino oscillations. As shown in Dighe & Smirnov (2000) and Takahashi et al. (2001), the mean energies of  $\nu_e$  and  $\bar{\nu}_e$  increase by the neutrino oscillations. This increase will raise the efficiency of the  ${}^7\text{Li}$  and  ${}^{11}\text{B}$  production. If we obtain some clear signals of neutrino oscillations in the abundances of  ${}^7\text{Li}$  and  ${}^{11}\text{B}$ , we would constrain the parameter values of neutrino oscillations from observations of light elements. This is a new procedure to constrain neutrino oscillation parameters completely different from the detections of supernova neutrinos.

In the present study, we investigate light element synthesis in supernova explosions taking account of the change of the neutrino spectra due to neutrino oscillations. We also evaluate the dependence of the yields of  ${}^7\text{Li}$  and  ${}^{11}\text{B}$  in the supernova ejecta on the mixing angle  $\sin^2 2\theta_{13}$  and mass hierarchy.

We set the luminosity and the energy spectrum of each flavor of neutrinos just emitted from a proto-neutron star in §2. We also set the parameter values of neutrino oscillations from the results of recent neutrino experiments. We explain a supernova explosion model and a nuclear reaction network for light element synthesis. We mention the cross sections of

charged-current reactions of the  $\nu$ -process to evaluate the reaction rates including neutrino oscillations. In §3, we show the transition probabilities of neutrino flavors with different values of  $\sin^2 2\theta_{13}$  and mass hierarchy. We also discuss the effect of the oscillations on the reaction rates of charged-current  $\nu$ -process reactions. In §4, we show the calculated mass fraction distribution of  ${}^7\text{Li}$  and  ${}^{11}\text{B}$  taking account of neutrino oscillations. Then, we show the dependence of the  ${}^7\text{Li}$  and  ${}^{11}\text{B}$  yields on  $\sin^2 2\theta_{13}$  and mass hierarchy. We also show the dependence on the temperatures of  $\nu_e$  and  $\bar{\nu}_e$  just emitted from proto-neutron star. In §5, we discuss the neutrino oscillations with supernova shock propagation and show the change of the  ${}^7\text{Li}$  and  ${}^{11}\text{B}$  yields by this effect. We also discuss the  ${}^7\text{Li}$  and  ${}^{11}\text{B}$  yields related to observations of stars which have traces of supernova explosions and supernova remnants. Finally, we conclude our study in §6.

## 2. Supernova Model and Parameters

### 2.1. Models of Supernova Neutrinos Emitted from a Proto-Neutron Star

We use a model of supernova neutrinos just emitted from a proto-neutron star based on the models in previous studies on the  $\nu$ -process nucleosynthesis (Yoshida et al. 2004, 2005, 2006). We here set up the energy spectra of three flavors of neutrinos when they just emitted from the proto-neutron star before they have been affected by neutrino oscillations in passing through the envelope. The neutrino luminosity is assumed to decrease exponentially with the decay time of  $\tau_\nu = 3$  s (after Woosley et al. 1990). The total neutrino energy  $E_\nu$  is set to be  $3.0 \times 10^{53}$  ergs which is almost equal to the gravitational binding energy of a  $1.4 M_\odot$  neutron star (e.g., Lattimer & Prakash 2001). The neutrino luminosity is equally partitioned for each flavor of neutrinos. The neutrino energy spectra are assumed to obey Fermi-Dirac (FD) distributions with zero-chemical potentials, similarly to previous studies on the  $\nu$ -process. The influence of nonzero chemical potentials has been discussed in Yoshida et al. (2005). The temperature of  $\nu_{\mu,\tau}$  and  $\bar{\nu}_{\mu,\tau}$ ,  $T_{\nu_{\mu,\tau}}$ , is set to be 6.0 MeV. This neutrino temperature is adopted so that the production of  ${}^{11}\text{B}$  from supernovae satisfies appropriate for GCE constraint on the light elements (Yoshida et al. 2005). The temperatures of  $\nu_e$  and  $\bar{\nu}_e$ ,  $T_{\nu_e}$  and  $T_{\bar{\nu}_e}$ , are set to be 3.2 MeV and 5.0 MeV, with which we have investigated light element synthesis and the  $r$ -process heavy element synthesis (Yoshida et al. 2004). We investigate detailed influences of neutrino oscillations using this set of neutrino temperatures.

We also use the temperature of 4.0 MeV for  $\nu_e$  and  $\bar{\nu}_e$ , which has been adopted in Woosley & Weaver (1995), Rauscher et al. (2002), and others. It has been indicated that the cooling of proto-neutron stars makes the temperatures of each flavor of neutrinos closer to each other (e.g., Keil et al. 2003). Therefore, we consider the case of  $T_{\nu_e}$  and  $T_{\bar{\nu}_e}$  to be 4.0

MeV and 5.0 MeV, respectively, too. For comparison, we set  $T_{\nu_e}$  and  $T_{\bar{\nu}_e}$  as 3.2 MeV and 4.0 MeV, corresponding to the case where only  $T_{\bar{\nu}_e}$  is changed.

## 2.2. Parameters for Neutrino Oscillations

In the present study, we consider the change of the neutrino spectra due to 3-flavor neutrino oscillations

$$i\hbar c \frac{d}{dx} \begin{pmatrix} \nu_e \\ \nu_\mu \\ \nu_\tau \end{pmatrix} = \left\{ U \begin{pmatrix} 0 & 0 & 0 \\ 0 & \frac{\Delta m_{21}^2 c^4}{2\varepsilon_\nu} & 0 \\ 0 & 0 & \frac{\Delta m_{31}^2 c^4}{2\varepsilon_\nu} \end{pmatrix} U^\dagger + \begin{pmatrix} \pm\sqrt{2}G_F(\hbar c)^3 \frac{\rho Y_e}{m_u} & 0 & 0 \\ 0 & 0 & 0 \\ 0 & 0 & 0 \end{pmatrix} \right\} \begin{pmatrix} \nu_e \\ \nu_\mu \\ \nu_\tau \end{pmatrix}, \quad (1)$$

$$U = \begin{pmatrix} c_{12}c_{13} & s_{12}c_{13} & s_{13} \\ -s_{12}c_{23} - c_{12}s_{23}s_{13} & c_{12}c_{23} - s_{12}s_{23}s_{13} & s_{23}c_{13} \\ s_{12}s_{23} - c_{12}c_{23}s_{13} & -c_{12}s_{23} - s_{12}c_{23}s_{13} & c_{23}c_{13} \end{pmatrix}, \quad (2)$$

where  $\Delta m_{ij}^2 = m_i^2 - m_j^2$ ,  $m_i$  is the mass of  $i$ -eigenstate neutrinos,  $\varepsilon_\nu$  is the neutrino energy,  $G_F$  is Fermi constant,  $\rho$  is the density,  $Y_e$  is electron fraction,  $m_u$  is the atomic mass unit,  $s_{ij} = \sin \theta_{ij}$ , and  $c_{ij} = \cos \theta_{ij}$ . Positive and negative signs in the potential term  $\pm\sqrt{2}G_F(\hbar c)^3 \rho Y_e/m_u$  correspond to the cases of neutrinos and antineutrinos. In this formulation the squared mass differences and the mixing angles are parameters. The values of these parameters except  $\theta_{13}$  and the sign of  $\Delta m_{31}^2$  have been precisely determined from recent neutrino experiments by Super-Kamiokande (Ashie et al. 2004), SNO (Ahmed et al. 2004), and KamLAND (Araki et al. 2005). We assume the mass differences and the mixing angles as follows:

$$\Delta m_{21}^2 = 7.9 \times 10^{-5} \text{ eV}^2 \quad \text{and} \quad \Delta m_{31}^2 = \pm 2.4 \times 10^{-3} \text{ eV}^2 \quad (3)$$

and

$$\sin^2 2\theta_{12} = 0.816 \quad \text{and} \quad \sin^2 2\theta_{23} = 1.0. \quad (4)$$

This parameter set corresponds to the LMA solution of neutrino oscillations. The sign of  $\Delta m_{31}^2$  has not been determined from recent neutrino experiments. Thus, we consider both normal mass hierarchy and inverted mass hierarchy. The positive value and the negative value of  $\Delta m_{31}^2$  correspond to normal mass hierarchy, i.e.,  $m_1 < m_2 < m_3$ , and inverted mass hierarchy, i.e.,  $m_3 < m_1 < m_2$ , respectively. From CHOOZ experiment (Apollonio et al. 2003) only upper limit of  $\sin^2 2\theta_{13}$  has been determined. We investigate the influence of changing  $\theta_{13}$  in the range of

$$0 \leq \sin^2 2\theta_{13} \leq 0.1. \quad (5)$$

### 2.3. Supernova Explosion Model

We calculate light element nucleosynthesis using the same supernova explosion model adopted in our previous studies (Yoshida et al. 2004, 2005). The presupernova model is 14E1 model, which is a  $16.2 M_{\odot}$  star just before the supernova explosion and corresponds to SN 1987A (Shigeyama & Nomoto 1990). The shock propagation of the supernova is calculated using a piecewise parabolic method code (Colella & Woodward 1984; Shigeyama et al. 1992). The explosion energy is set to be  $1 \times 10^{51}$  ergs. The mass cut is located at  $1.61 M_{\odot}$ . Note that it is not needed to calculate the structure inside the mass cut. In the present study, we calculate neutrino oscillations with the density structure of the presupernova model. When the shock front is in inner high density region, there is no influence of the shock propagation to the neutrino oscillations. This is because the oscillation amplitude is too small despite the presence of the shock wave in such a high density region. Its effect will be discussed in detail in §5.

### 2.4. Nuclear Reaction Network for the $\nu$ -Process with Neutrino Oscillations

Our nuclear reaction network consists of 291 species of nuclei from  $n$ ,  $p$ , to Ge. The included nuclear species and their associated nuclear reactions are the same as those in Yoshida et al. (2004), except charged-current  $\nu$ -process reactions on  ${}^4\text{He}$  and  ${}^{12}\text{C}$ , which will be discussed later in this subsection. The rates of neutral-current  $\nu$ -process reactions and those of the other charged-current reactions are adopted from the rates with the assumption of FD distribution of the neutrino spectra. As mentioned in Introduction, the rates of the neutral-current reactions do not change by neutrino oscillations.

When we consider neutrino oscillations, the energy spectra of  $\nu_e$  and  $\bar{\nu}_e$  emitted from a proto-neutron star change from FD distributions and charged-current  $\nu$ -process reaction rates are not merely simple functions of neutrino temperatures. In such a condition, we need to evaluate a neutrino flux as a function of the neutrino energy. The number flux of  $i$ -flavor neutrinos ( $i = e, \mu, \tau$ ) emitted from the proto-neutron star with the energy of  $\varepsilon_{\nu}$  can be written as

$$\frac{d\phi_{\nu_i}}{d\varepsilon_{\nu}} = \frac{L_{\nu_i}}{4\pi r^2} \frac{1}{F_3(\eta_{\nu_i})(kT_{\nu_i})^4} \frac{\varepsilon_{\nu}^2}{\exp(\frac{\varepsilon_{\nu}}{kT_{\nu_i}} - \eta_{\nu_i}) + 1} \quad (6)$$

and

$$F_3(\eta_{\nu_i}) = \int_0^{\infty} \frac{x^3 dx}{\exp(x - \eta_{\nu_i}) + 1}, \quad (7)$$

where  $L_{\nu_i}$  is the luminosity of  $i$ -flavor neutrinos,  $r$  is the radius,  $k$  is the Boltzmann constant,  $T_{\nu_i}$  is the neutrino temperature, and  $\eta_{\nu_i}$  is the degeneracy factor (e.g., Balantekin & Yüksel

2005). Here we define  $P_{ij}(r; \varepsilon_\nu)$  as the oscillation probability from  $i$ -flavor to  $j$ -flavor at the radius of  $r$  and the energy of  $\varepsilon_\nu$ . Taking the cross section of a  $\nu$ -process reaction as a function of  $\varepsilon_\nu$ ,  $\sigma_{\nu_e}(\varepsilon_\nu)$ , we evaluate the reaction rate with neutrino oscillations  $\lambda_{\nu_e}$  as

$$\lambda_{\nu_e} = \sum_{i=e,\mu,\tau} \frac{L_{\nu_i}}{4\pi r^2} \frac{1}{F_3(\eta_{\nu_i})(kT_{\nu_i})^4} \int_0^\infty \frac{\varepsilon_\nu^2 P_{ie}(r; \varepsilon_\nu) \sigma_{\nu_e}(\varepsilon_\nu)}{\exp(\frac{\varepsilon_\nu}{kT_{\nu_i}} - \eta_{\nu_i}) + 1} d\varepsilon_\nu. \quad (8)$$

In the present study, we consider the effect on neutrino oscillations for charged-current reactions of  ${}^4\text{He}$ ,  ${}^4\text{He}(\nu_e, e^- p){}^3\text{He}$  and  ${}^4\text{He}(\bar{\nu}_e, e^+ n){}^3\text{H}$ , and the reactions of  ${}^{12}\text{C}$ ,  ${}^{12}\text{C}(\nu_e, e^- p){}^{11}\text{C}$ ,  ${}^{12}\text{C}(\nu_e, e^- \gamma){}^{12}\text{N}$ ,  ${}^{12}\text{C}(\bar{\nu}_e, e^+ n){}^{11}\text{B}$ , and  ${}^{12}\text{C}(\bar{\nu}_e, e^+ \gamma){}^{12}\text{B}$ . However, the detailed data of the cross sections of these reactions as functions of  $\varepsilon_\nu$  have not been reported and one can find only energy averaged reaction rates as functions of neutrino temperature. Therefore, we adopt analytical approximation to the cross sections with respect to  $\varepsilon_\nu$  as

$$\sigma_{\nu_e}(\varepsilon_\nu) = \begin{cases} a(\varepsilon_\nu - \varepsilon_{th})^b & \text{for } \varepsilon_\nu \geq \varepsilon_{th}, \\ 0 & \text{for } \varepsilon_\nu < \varepsilon_{th}, \end{cases} \quad (9)$$

where  $\varepsilon_{th}$  is the threshold energy of each reaction. Coefficients are determined so as to fit the rate of the corresponding reaction with the assumption of the FD distributions to the values tabulated in the 1992 work by R. D. Hoffman & S. E. Woosley, HW92<sup>1</sup>. The coefficients and the thresholds are listed in Table 1. When we evaluate the reaction rates from the cross sections with assumptions of the FD distributions, these values are in reasonable agreement with those of HW92 within  $\pm 9\%$ .

### 3. Neutrino Oscillations in Presupernovae

In order to evaluate the reaction rates of the charged-current  $\nu$ -process reactions with neutrino oscillations, we numerically solve the oscillations of the neutrinos passing through a presupernova star in Runge-Kutta method and based on analytical expression of Kimura, Takamura, & Yokomakura (2002a,b). We use the density profile of 14E1 model of Shigeyama & Nomoto (1990). The density profile is shown in Fig. 1 in Shigeyama & Nomoto (1990).

When neutrinos pass through the stellar interior, there are resonances of neutrino oscillations where the transition probabilities change largely. The resonance density  $\rho_{\text{res}}$  is determined from the squared mass difference and the neutrino energy. The resonance density is written as

$$\rho_{\text{res}} Y_e = \frac{m_u \Delta m_{ji}^2 c^4 \cos 2\theta_{ij}}{2\sqrt{2} G_F (\hbar c)^3 \varepsilon_\nu} = 6.55 \times 10^6 \left( \frac{\Delta m_{ji}^2}{1 \text{ eV}^2} \right) \left( \frac{1 \text{ MeV}}{\varepsilon_\nu} \right) \cos 2\theta_{ij} \text{ g cm}^{-3}. \quad (10)$$

---

<sup>1</sup>[http://www-phys.llnl.gov/Research/RRSN/nu\\_csbr/neu\\_rate.html](http://www-phys.llnl.gov/Research/RRSN/nu_csbr/neu_rate.html).

Electron number density  $n_e$  relates to the density and electron fraction through  $n_e = \rho Y_e / m_u$ . The transition probabilities depend on the adiabaticity of the resonance strongly. The adiabaticity is estimated using the adiabaticity parameter  $\gamma$ . The flip probability  $P_f$ , which means the probability that a neutrino in one mass eigenstate changes to another mass eigenstate is written as (e.g., Dighe & Smirnov 2000)

$$P_f = \exp\left(-\frac{\pi}{2}\gamma\right) \quad (11)$$

and

$$\gamma = \frac{\Delta m_{ji}^2 c^3 \sin^2 2\theta_{ij}}{2\hbar\varepsilon_\nu \cos 2\theta_{ij}} \left| \frac{1}{(1/n_e)(dn_e/dr)} \right|. \quad (12)$$

When  $\gamma \gg 1$ , i.e., the flip probability  $P_f$  is very small ( $P_f \ll 1$ ), the resonance is adiabatic. When the flip probability is close to unity, the resonance is nonadiabatic.

Figure 1 shows the transition probability of  $\nu_e$  to  $\nu_e$ ,  $P_{ee}$ , the sum of the transition probabilities of  $\nu_\mu \rightarrow \nu_e$  and  $\nu_\tau \rightarrow \nu_e$ ,  $P_{xe}$ , and the corresponding transition probabilities for antineutrinos  $P_{\text{eeb}}$  and  $P_{\text{xeb}}$  in the case of  $\varepsilon_\nu = 50$  MeV and normal mass hierarchy. There are resonances of  $\Delta m_{31}^2$  and  $\theta_{13}$ , which is called H-resonance, at  $\rho_{\text{res}} = 6.3 \times 10^2$  g cm<sup>-3</sup> and of  $\Delta m_{21}^2$  and  $\theta_{12}$ , which is called L-resonance, at  $\rho_{\text{res}} = 8.9$  g cm<sup>-3</sup>. The H-resonance is located in innermost region of the He/C layer ( $\sim 3.8M_\odot$ ) and the L-resonance is in the He/C layer ( $\sim 5.4M_\odot$ ). Both of H- and L-resonances appear for neutrinos and do not appear for antineutrinos. The adiabaticity of H-resonance depends on the value of  $\sin^2 2\theta_{13}$ . L-resonance is always adiabatic in our parameter set. We see in the mass coordinate range of  $M_r \lesssim 3.8M_\odot$  that the amplitude of neutrino oscillation is very small and that the flavor exchange practically does not occur for both neutrinos and antineutrinos.

In the mass coordinate region of  $M_r \gtrsim 3.8M_\odot$ , the characteristics of the transition probabilities depend on mass hierarchy and the adiabaticity of H-resonance. In the case of  $\sin^2 2\theta_{13} = 1 \times 10^{-2}$  (see Fig. 1a), H-resonance appears for neutrinos and is adiabatic. The transition from  $\nu_e$  to  $\nu_{\mu,\tau}$  occurs completely, i.e.,  $P_{ee}$  becomes almost zero in the He/C layer. At the same time, the transition probability from  $\nu_\mu$  or  $\nu_\tau$  to  $\nu_e$  becomes large, i.e.,  $P_{xe}$  is close to 1. On the other hand, there is no resonance for antineutrinos. The transition probabilities  $P_{\text{eeb}}$  and  $P_{\text{xeb}}$  gradually change in the He/C layer, and about 30% of antineutrinos change flavors.

In the case of  $\sin^2 2\theta_{13} = 1 \times 10^{-6}$  (see Fig. 1b), H-resonance is nonadiabatic. So, complete change from  $\nu_e$  to  $\nu_{\mu,\tau}$  does not occur. The transition probabilities for neutrinos change gradually as a function of the mass coordinate similarly to antineutrinos. Finally, about 70% of neutrinos change flavors. The transition probabilities for antineutrinos are the same as the case of  $\sin^2 2\theta_{13} = 1 \times 10^{-2}$ .



Figure 2 shows the transition probabilities in the case of inverted mass hierarchy. In this case, H-resonance appears for antineutrinos. When  $\sin^2 2\theta_{13}$  is equal to  $1 \times 10^{-2}$  (see Fig. 2a), H-resonance is adiabatic and almost all  $\bar{\nu}_e$  change to  $\bar{\nu}_\mu$  and  $\bar{\nu}_\tau$ . The transition probability  $P_{\text{xeb}}$  also becomes close to unity. On the other hand, neutrinos change their flavors gradually in the He-layer because of no appearance of H-resonance. When  $\sin^2 2\theta_{13}$  is equal to  $1 \times 10^{-6}$ , H-resonance is nonadiabatic. The change of the transition probabilities with increasing the mass coordinate is the same as that in the case of normal mass hierarchy and the nonadiabatic H-resonance. In the case of nonadiabatic resonance, the flavor change occurs as if there is no resonance.

The increase in charged-current  $\nu$ -process reaction rates strongly depends on the adiabaticity of H-resonance. If H-resonance is adiabatic, the reaction rates of charged-current reactions for  $\nu_e$  (normal mass hierarchy) and  $\bar{\nu}_e$  (inverted mass hierarchy) become much larger than those without the oscillations in the He-layer. If H-resonance is nonadiabatic, the increase in the rates of corresponding charged-current reactions would be much smaller. Therefore, the adiabaticity of H-resonance affects the final yields of  ${}^7\text{Li}$  and  ${}^{11}\text{B}$ .

We note that the shock propagation effect on neutrino oscillations in supernova ejecta is not considered in this study. We do not consider that the change of neutrino oscillations due to the shock propagation would change the yields of  ${}^7\text{Li}$  and  ${}^{11}\text{B}$ . When neutrinos pass through the O/Ne layer, the amplitude of neutrino oscillations is very small because the density profile, where the density is much larger than H-resonance density, does not affect neutrino oscillations. Thus, when the shock wave moves inside the O/C layer, the shock wave does not affect the transition probabilities of neutrinos and antineutrinos even if we consider the shock propagation. After the shock wave arrives at the O/C layer, the shock wave will change the transition probabilities. We set the decay time of the neutrino flux to be 3 s which is to be compared with the shock arrival time to the O/C layer about 5 s. Because of this time lag, more than 80% of neutrinos pass through the supernova ejecta before the shock arrives at the O/C layer. We will discuss the influence of the shock wave on neutrino oscillations in the supernova in §5.

## 4. Yields of ${}^7\text{Li}$ and ${}^{11}\text{B}$

### 4.1. Mass Fraction Distributions of ${}^7\text{Li}$ and ${}^{11}\text{B}$

We show the change of the mass fractions of  ${}^7\text{Li}$  and  ${}^{11}\text{B}$  due to neutrino oscillations. Figure 3 shows the mass fraction distributions of  ${}^7\text{Li}$  and  ${}^{11}\text{B}$ . Panels (a) and (b) correspond to the case of normal mass hierarchy, and panels (c) and (d) correspond to inverted mass

hierarchy. In these figures we show the mass fraction distributions of  ${}^7\text{Li}$  and its isobar  ${}^7\text{Be}$  separately. The mass fraction distributions of  ${}^{11}\text{B}$  and  ${}^{11}\text{C}$  are also drawn separately.

Let us first discuss the case of normal mass hierarchy and  $\sin^2 2\theta_{13} = 1 \times 10^{-2}$  (adiabatic H-resonance for neutrinos) shown by thick lines in Figs. 3a and 3b. We find the increase in the mass fractions of  ${}^7\text{Li}$ ,  ${}^7\text{Be}$ ,  ${}^{11}\text{B}$ , and  ${}^{11}\text{C}$  compared with those without the neutrino oscillations in the He layer. The mass fraction of  ${}^7\text{Li}$  with the neutrino oscillations is larger by about a factor of 1.2 than that without the oscillations in most region of the He layer (see Fig. 3a). In the range of  $4.3M_\odot \lesssim M_r \lesssim 4.6M_\odot$ , the increment degree is larger. In the O-rich layers of  $M_r \lesssim 3.8M_\odot$ , we do not see any clear differences due to neutrino oscillations in the mass fraction. The transition probabilities to other neutrino flavors are very small because of high density in this region (see Fig. 1). The obtained yield of  ${}^7\text{Li}$  is  $1.79 \times 10^{-7}M_\odot$ . When we do not consider neutrino oscillations, the yield is  $1.50 \times 10^{-7}M_\odot$ . The yield of  ${}^7\text{Li}$  increases by a factor of 1.19 owing to the neutrino oscillations.

The mass fraction of  ${}^7\text{Be}$  is larger by about a factor of 2.5 than that without the neutrino oscillations in the innermost region of the He layer,  $3.8M_\odot \lesssim M_r \lesssim 4.3M_\odot$  (see Fig. 3a). In the range of  $4.3M_\odot \lesssim M_r \lesssim 4.6M_\odot$ , where the  ${}^7\text{Be}$  mass fraction increases with the mass coordinate, the increase in the  ${}^7\text{Be}$  mass fraction due to the neutrino oscillations is more than a factor of 3. In the range of  $M_r \gtrsim 4.6M_\odot$  it is a factor of  $2.5 \sim 3.2$ . Finally, the obtained yield of  ${}^7\text{Be}$  is  $2.66 \times 10^{-7}M_\odot$ . Without the neutrino oscillations, the yield of  ${}^7\text{Be}$  is  $8.62 \times 10^{-8}M_\odot$ . The yield of  ${}^7\text{Be}$  increases by a factor of 3.1 owing to the neutrino oscillations. Thus, the total yield of  ${}^7\text{Li}$ , the sum of the yields of  ${}^7\text{Li}$  and  ${}^7\text{Be}$ , is  $4.45 \times 10^{-7}M_\odot$  with the neutrino oscillations and  $2.36 \times 10^{-7}M_\odot$  without the oscillations. The  ${}^7\text{Li}$  yield with the neutrino oscillations is larger by a factor of 1.89 than that without the oscillations.

The mass fraction of  ${}^{11}\text{B}$  in the range of  $M_r \gtrsim 4.3M_\odot$  of the He layer is larger by about a factor of  $1.2 \sim 1.3$  than that without the oscillations (see Fig. 3b). Inside the range of the He layer, it increases by about a factor of 2.1. The increase in the mass fraction of  ${}^{11}\text{C}$  in the He layer is about a factor of  $3.4 \sim 3.9$ . This increase is larger than that of  ${}^{11}\text{B}$  and is close to the factor of  ${}^7\text{Be}$ . The  ${}^{11}\text{B}$  and  ${}^{11}\text{C}$  mass fractions in the O-rich layers of  $M_r \lesssim 3.8M_\odot$  are not affected strongly by the neutrino oscillations. The yields of  ${}^{11}\text{B}$  and  ${}^{11}\text{C}$  in this case are  $7.02 \times 10^{-7}M_\odot$  and  $9.16 \times 10^{-8}M_\odot$ . Without the neutrino oscillations, the corresponding yields are  $5.63 \times 10^{-7}M_\odot$  and  $6.29 \times 10^{-8}M_\odot$ . Thus, the total  ${}^{11}\text{B}$  yield increases by a factor of 1.27.

We discuss the production process of  ${}^7\text{Li}$  and  ${}^{11}\text{B}$  in the He layer and the effect of the neutrino oscillations on the  $\nu$ -process reactions. In the He layer,  ${}^7\text{Li}$  and  ${}^7\text{Be}$  are produced through  ${}^4\text{He}(\nu, \nu'p){}^3\text{H}(\alpha, \gamma){}^7\text{Li}$  and  ${}^4\text{He}(\nu, \nu'n){}^3\text{He}(\alpha, \gamma){}^7\text{Be}$ , respectively. The corresponding charged-current  $\nu$ -process reactions are  ${}^4\text{He}(\bar{\nu}_e, e^+n){}^3\text{H}(\alpha, \gamma){}^7\text{Li}$  and  ${}^4\text{He}(\nu_e, e^-p){}^3\text{He}(\alpha, \gamma){}^7\text{Be}$ .

Most of  $^{11}\text{B}$  is produced through  ${}^7\text{Li}(\alpha, \gamma){}^{11}\text{B}$  and the contribution from  ${}^{12}\text{C}(\nu, \nu'p){}^{11}\text{B}$  is small. The  $^{11}\text{B}$  in the O-rich layers is also produced from  ${}^{12}\text{C}$ . The  ${}^{11}\text{C}$  is produced through  ${}^{12}\text{C}(\nu, \nu'n){}^{11}\text{C}$ . The charged-current  $\nu$ -process reactions from  ${}^{12}\text{C}$  are  ${}^{12}\text{C}(\bar{\nu}_e, e^+n){}^{11}\text{B}$  and  ${}^{12}\text{C}(\nu_e, e^-p){}^{11}\text{C}$ . Main production processes of these light elements are also written in Yoshida et al. (2004, 2005, 2006). In the case of normal mass hierarchy and adiabatic H-resonance for neutrinos,  $\nu_e$  and  $\nu_{\mu,\tau}$  are completely exchanged owing to the adiabatic mixing, and therefore the rates of  ${}^4\text{He}(\nu_e, e^-p){}^3\text{He}$  and  ${}^{12}\text{C}(\nu_e, e^-p){}^{11}\text{C}$  increase. Thus, the mass fractions of  ${}^7\text{Be}$  and  ${}^{11}\text{C}$  become larger. On the other hand, there are no resonances for antineutrinos. The transition probability between  $\bar{\nu}_e$  and  $\bar{\nu}_{\mu,\tau}$  is small so that the rates of  ${}^4\text{He}(\bar{\nu}_e, e^+n){}^3\text{H}$  and  ${}^{12}\text{C}(\nu_e, e^-p){}^{11}\text{C}$  scarcely become larger, and therefore the increase in the mass fractions of  ${}^7\text{Li}$  and  ${}^{11}\text{B}$  is small. The increase by a factor of 2 in the mass fraction of  ${}^{11}\text{B}$  is due to the production by way of  ${}^7\text{Be}(n, p){}^7\text{Li}(\alpha, \gamma){}^{11}\text{B}$ .

Secondly, we consider the case of normal mass hierarchy and  $\sin^2 2\theta_{13} = 1 \times 10^{-6}$  (non-adiabatic H-resonance for neutrinos) shown by thin lines in Figs. 3a and 3b. The increment degree of  ${}^7\text{Li}$  mass fraction compared with the case without the neutrino oscillations becomes gradually larger with increasing the mass coordinate (see Fig. 3a). The maximum increment degree is 1.3 at the outer edge of the He layer. The mass fraction of  ${}^7\text{Be}$  is larger by a factor of 1.2 compared with the case without the neutrino oscillations where the mass fraction has the maximum value. The increment degree becomes larger with increasing the mass coordinate, but the mass fraction is much smaller there. Thus, the obtained yields of  ${}^7\text{Li}$  and  ${}^7\text{Be}$  are  $1.65 \times 10^{-7}M_\odot$  and  $1.02 \times 10^{-7}M_\odot$ . The total yield of  ${}^7\text{Li}$  is  $2.67 \times 10^{-7}M_\odot$ ; it is larger by a factor of only 1.13 than the case without the neutrino oscillations.

The increment degree of the  ${}^{11}\text{B}$  mass fraction due to the neutrino oscillations gradually increases with the mass coordinate in the He layer (see Fig. 3b). However, increment degree is 1.2 at the maximum at the outer edge of the He layer. This is due to smaller transition probability from  $\bar{\nu}_{\mu,\tau}$  to  $\bar{\nu}_e$  (see Fig. 1b). The dependence of increasing  ${}^{11}\text{C}$  mass fraction on the mass coordinate is similar to that of  ${}^{11}\text{B}$ . The maximum increment degree is 2.9. The obtained yields of  ${}^{11}\text{B}$  and  ${}^{11}\text{C}$  are  $5.75 \times 10^{-7}M_\odot$  and  $6.47 \times 10^{-8}M_\odot$  and, therefore, the total  ${}^{11}\text{B}$  yield is  $6.40 \times 10^{-7}M_\odot$ . It is only slightly larger by a factor of 1.02 compared with the case without the oscillations.

Thirdly, we consider the case of inverted mass hierarchy and  $\sin^2 2\theta_{13} = 1 \times 10^{-2}$  (adiabatic H-resonance for antineutrinos) shown by thick lines in Figs. 3c and 3d. The mass fraction of  ${}^7\text{Li}$  is larger by a factor of  $1.4 \sim 1.5$  in most region of the He layer. For  ${}^{11}\text{B}$ , the mass fraction increases by a factor of  $1.1 \sim 1.4$ . The yields of  ${}^7\text{Li}$  and  ${}^{11}\text{B}$  are  $2.22 \times 10^{-7}M_\odot$  and  $7.05 \times 10^{-7}M_\odot$ . Compared with those without the oscillations, these yields are larger by factors of 1.48 and 1.25. Although adiabatic H-resonance appears for antineutrinos and,

therefore, the flavor change between  $\bar{\nu}_e$  and  $\bar{\nu}_{\mu,\tau}$  occurs completely, the increment degree of the  ${}^7\text{Li}$  and  ${}^{11}\text{B}$  mass fractions are smaller than those of  ${}^7\text{Be}$  and  ${}^{11}\text{C}$  in the corresponding case of normal mass hierarchy. This is because the difference between the mean energies for  $\bar{\nu}_e$  and  $\bar{\nu}_{\mu,\tau}$  is smaller than that for  $\nu_e$  and  $\nu_{\mu,\tau}$ . This small difference of the mean neutrino energies causes smaller enhancement of  ${}^7\text{Li}$  and  ${}^{11}\text{B}$  even in the adiabatic mixing.

The mass fractions of  ${}^7\text{Be}$  and  ${}^{11}\text{C}$  are larger than those without the neutrino oscillations in the range of  $M_r \gtrsim 4.8M_\odot$  in the He layer. On the other hand, they are smaller than those without the neutrino oscillations inside the region. This is because neutrons produced through  ${}^4\text{He}(\bar{\nu}_e, e^+n){}^3\text{H}$ , of which rate is enhanced by the neutrino oscillations, decompose  ${}^3\text{He}$ ,  ${}^7\text{Be}$ , and  ${}^{11}\text{C}$ . The yields of  ${}^7\text{Be}$  and  ${}^{11}\text{C}$  are  $8.20 \times 10^{-8}M_\odot$  and  $6.35 \times 10^{-8}M_\odot$ . The yield ratios to the case without the neutrino oscillations are 0.95 and 1.01 for  ${}^7\text{Be}$  and  ${}^{11}\text{C}$ . The total yields of  ${}^7\text{Li}$  and  ${}^{11}\text{B}$  are  $3.04 \times 10^{-7}M_\odot$  and  $7.69 \times 10^{-7}M_\odot$ , and their increment factors are 1.29 and 1.23.

Finally, we show the case of inverted mass hierarchy and  $\sin^2 2\theta_{13} = 1 \times 10^{-6}$  (nonadiabatic H-resonance for antineutrinos) represented by thin lines in Figs. 3c and 3d. The mass fraction distributions of all four nuclear species are the same as the corresponding distributions in the case of normal mass hierarchy and nonadiabatic H-resonance. We showed in §3 that the exchange probabilities for  $\nu_e(\bar{\nu}_e) \rightarrow \nu_e(\bar{\nu}_e)$  and  $\nu_e(\bar{\nu}_e) \rightarrow \nu_{\mu,\tau}(\bar{\nu}_{\mu,\tau})$  are identical in the cases of nonadiabatic H-resonance independent of mass hierarchy at  $\varepsilon_\nu = 50$  MeV. The same conclusion is inferred for neutrinos at different neutrino energies.

## 4.2. Yields of ${}^7\text{Li}$ and ${}^{11}\text{B}$

In this subsection we discuss detailed dependence of the  ${}^7\text{Li}$  and  ${}^{11}\text{B}$  yields on the mass hierarchy and  $\sin^2 2\theta_{13}$ . When we do not consider neutrino oscillations, the calculated yields of  ${}^7\text{Li}$  and  ${}^{11}\text{B}$  are  $2.36 \times 10^{-7}$  and  $6.26 \times 10^{-7}M_\odot$ . We evaluate the ratios of the  ${}^7\text{Li}$  and  ${}^{11}\text{B}$  yields with and without neutrino oscillations.

Figure 4 shows the dependence of the yield ratios of  ${}^7\text{Li}$  (a) and  ${}^{11}\text{B}$  (b) on  $\sin^2 2\theta_{13}$  in the range between  $1 \times 10^{-6}$  and  $1 \times 10^{-1}$ . We find three characteristics of the  ${}^7\text{Li}$  and  ${}^{11}\text{B}$  yields as to the dependence on  $\sin^2 2\theta_{13}$ . In the case of  $\sin^2 2\theta_{13} \lesssim 2 \times 10^{-5}$ , the  ${}^7\text{Li}$  and  ${}^{11}\text{B}$  yield ratios keep constant values and do not depend on mass hierarchy. In the range of  $2 \times 10^{-5} \lesssim \sin^2 2\theta_{13} \lesssim 2 \times 10^{-3}$ , the  ${}^7\text{Li}$  and  ${}^{11}\text{B}$  yield ratios increase with  $\sin^2 2\theta_{13}$ . The difference due to mass hierarchy is also seen. In the range of  $\sin^2 2\theta_{13} \gtrsim 2 \times 10^{-3}$ , the yield ratios roughly keep constant values again. The difference due to mass hierarchy is also seen in this range. The above dependence is compared with that of the adiabaticity parameter

$\gamma$  (see Eq. (10)) and the flip probability  $P_f$  (see eq. (11)) of H-resonance at the location of the resonance density. The value  $1 - P_f$  related to  $\sin^2 2\theta_{13}$  is also drawn in Fig. 4. We set the neutrino energy to be 50 MeV. This neutrino energy is close to the optimum energy contributing most strongly to the charged-current  $\nu$ -process reactions of  ${}^4\text{He}$ .

In the case of  $\sin^2 2\theta_{13} \lesssim 2 \times 10^{-5}$ ,  $1 - P_f$  is almost equal to 0; H-resonance is nonadiabatic. In the case of  $2 \times 10^{-5} \lesssim \sin^2 2\theta_{13} \lesssim 2 \times 10^{-3}$ ,  $1 - P_f$  increases with  $\sin^2 2\theta_{13}$ , i.e., the resonance changes from nonadiabatic to adiabatic with increasing  $\sin^2 2\theta_{13}$ . We call this range of  $\sin^2 2\theta_{13}$  “transition range”. In the case of  $\sin^2 2\theta_{13} \gtrsim 2 \times 10^{-3}$ , the value of  $1 - P_f$  is almost equal to 1, i.e., H-resonance is adiabatic. The change of the flip probability  $P_f$  as a function of  $\sin^2 2\theta_{13}$  is roughly similar to the change of the yields of  ${}^7\text{Li}$  and  ${}^{11}\text{B}$ . Thus, we conclude that the dependence of the  ${}^7\text{Li}$  and  ${}^{11}\text{B}$  yields on  $\sin^2 2\theta_{13}$  strongly correlates to the adiabaticity of H-resonance.

In the case of the nonadiabatic range,  $\sin^2 2\theta_{13} \lesssim 2 \times 10^{-5}$ , the  ${}^7\text{Li}$  and  ${}^{11}\text{B}$  yield ratios are about 1.1 and 1.02, respectively, and they are independent of mass hierarchy. In the limit of  $\sin^2 2\theta_{13} = 0$ , the yield ratios still stay near the above values. We showed in §3 that the transition probabilities do not depend on mass hierarchy in nonadiabatic region. This characteristics can also be seen in the  ${}^7\text{Li}$  and  ${}^{11}\text{B}$  yield ratios. The yield ratios 1.1 and 1.02 are slightly larger than unity, which reflect small enhancement of the mass fractions of  ${}^7\text{Li}$  and  ${}^{11}\text{B}$  in outer region of the He/C layer as shown in §4.1.

In the transition range, the yield ratios of  ${}^7\text{Li}$  and  ${}^{11}\text{B}$  increase with  $\sin^2 2\theta_{13}$  and a difference relating to mass hierarchy appears. The increase in the  ${}^7\text{Li}$  yield is due to the enhancement of the  ${}^7\text{Be}$  production through  ${}^4\text{He}(\nu_e, e^-p){}^3\text{He}(\alpha, \gamma){}^7\text{Be}$ . The increase in the  ${}^{11}\text{B}$  yield also arises from the enhancement of  ${}^7\text{Li}$  yield by way of  ${}^7\text{Be}$ .

In the adiabatic range, the  ${}^7\text{Li}$  yield ratio depends on mass hierarchy: the  ${}^7\text{Li}$  yield ratio is 1.9 in the case of normal mass hierarchy, and 1.3 in inverted mass hierarchy. As shown in §4.1, the increase in the reaction rate of  ${}^4\text{H}(\nu_e, e^-p){}^3\text{He}$  raises the  ${}^7\text{Be}$  production in normal mass hierarchy. The increase in the rate of  ${}^4\text{He}(\bar{\nu}_e, e^+n){}^3\text{H}$  also raises the  ${}^7\text{Li}$  production in inverted mass hierarchy. The increase in the reaction rate of  ${}^4\text{He}(\nu_e, e^-p){}^3\text{He}$  in normal mass hierarchy is larger than that of  ${}^4\text{He}(\bar{\nu}_e, e^+n){}^3\text{H}$  in inverted mass hierarchy. In the case of  $T_{\nu_e} = 6$  MeV, the reaction rate of  ${}^4\text{He}(\nu_e, e^-p){}^3\text{He}$  is larger than that of  ${}^4\text{He}(\bar{\nu}_e, e^+n){}^3\text{H}$ . Further, the difference between  $T_{\nu_e}$  and  $T_{\nu_{\mu,\tau}}$  is larger than that between  $T_{\bar{\nu}_e}$  and  $T_{\bar{\nu}_{\mu,\tau}}$  (where note that  $T_{\nu_{\mu,\tau}} = T_{\bar{\nu}_{\mu,\tau}}$ ). Thus, the increase in the  ${}^7\text{Li}$  yield ratio in normal mass hierarchy is larger than that in inverted mass hierarchy. The  ${}^{11}\text{B}$  yield ratio also depends on mass hierarchy, but the difference is smaller than that of the  ${}^7\text{Li}$  yield ratio. As mentioned above, the increase in the  ${}^{11}\text{B}$  yield arises in this case from enhanced  ${}^7\text{Li}$  production by way of  ${}^7\text{Be}$ . However, most of  ${}^7\text{Li}$  produced through  ${}^7\text{Be}$  do not capture  $\alpha$ -particles to form  ${}^{11}\text{B}$ .

### 4.3. Dependence on Initial $\nu_e$ and $\bar{\nu}_e$ Temperatures

In the present study we adopted the temperatures of  $\nu_e$ ,  $\bar{\nu}_e$ , and  $\nu_{\mu,\tau}$  ( $\bar{\nu}_{\mu,\tau}$ ) equal to 3.2 MeV, 5.0 MeV, and 6.0 MeV, respectively. On the other hand, some other studies (e.g. Woosley & Weaver 1995; Rauscher et al. 2002) adopted the temperature of  $\nu_e$  and  $\bar{\nu}_e$  as  $T_{\nu_e} = T_{\bar{\nu}_e} = 4.0$  MeV. Since the enhancement of the  ${}^7\text{Li}$  and  ${}^{11}\text{B}$  yields depends on the neutrino temperatures at the neutrino sphere, we can find some effects on different temperatures of  $\nu_e$  and  $\bar{\nu}_e$ . We consider four sets of the temperatures of  $\nu_e$  and  $\bar{\nu}_e$ :  $(T_{\nu_e}, T_{\bar{\nu}_e}) = (3.2 \text{ MeV}, 5 \text{ MeV})$ ,  $(4 \text{ MeV}, 4 \text{ MeV})$ ,  $(4 \text{ MeV}, 5 \text{ MeV})$ ,  $(3.2 \text{ MeV}, 4 \text{ MeV})$  as mentioned in §2.1. The first set is our standard model. The second set is the one adopted in Woosley & Weaver (1995), Rauscher et al. (2002), and so on. The third set satisfy  $T_{\nu_e} < T_{\bar{\nu}_e}$ , but the difference of the temperature is smaller than the first set. The fourth set is prepared for comparison to the other three models: either  $T_{\nu_e}$  or  $T_{\bar{\nu}_e}$  is different from the other sets. In these four sets we use a temperature of  $\nu_{\mu,\tau}$  and  $\bar{\nu}_{\mu,\tau}$ , 6.0 MeV. The  ${}^7\text{Li}$  and  ${}^{11}\text{B}$  yields without neutrino oscillations in the four cases of the neutrino temperatures are listed in Table 2.

Figure 5 shows the  ${}^7\text{Li}$  and  ${}^{11}\text{B}$  yield ratios as functions of  $\sin^2 2\theta_{13}$  in the above four cases of neutrino temperatures. In the case of normal mass hierarchy (see Fig. 5a), the  ${}^7\text{Li}$  yield ratio depends on initial temperatures in the nonadiabatic range, and the dependence becomes larger in the adiabatic range. In the case of small temperatures of  $\nu_e$  and  $\bar{\nu}_e$ , i.e.,  $(T_{\nu_e}, T_{\bar{\nu}_e}) = (3.2 \text{ MeV}, 4 \text{ MeV})$ , the  ${}^7\text{Li}$  yield ratio becomes 2.1 at the maximum. On the other hand, large neutrino temperature, i.e.,  $(T_{\nu_e}, T_{\bar{\nu}_e}) = (4 \text{ MeV}, 5 \text{ MeV})$ , provides the  ${}^7\text{Li}$  yield ratio of 1.8. In the adiabatic range, the final  ${}^7\text{Li}$  yield does not depend on the initial neutrino temperatures. The difference is due to the difference of the  ${}^7\text{Li}$  yields without neutrino oscillations. After the neutrino mixing at H-resonance, the  $\nu_e$  energy spectrum becomes FD distribution with  $T_{\nu_e} = 6 \text{ MeV}$ , independent of the initial  $T_{\nu_e}$ . In addition, the yield produced originally as  ${}^7\text{Be}$  is much larger than the  ${}^7\text{Li}$  yield produced without neutrino oscillations. Therefore, the  ${}^7\text{Be}$  yield does not depend strongly on the neutrino temperatures among the four sets.

In the case of inverted mass hierarchy (see Fig. 5b), the dependence of the  ${}^7\text{Li}$  yield ratio on the initial neutrino temperatures is similar to that in normal mass hierarchy. The yield ratio is about 1.4 in the case of  $(T_{\nu_e}, T_{\bar{\nu}_e}) = (3.2 \text{ MeV}, 4 \text{ MeV})$  and in the adiabatic range. It is 1.26 in the case of  $(T_{\nu_e}, T_{\bar{\nu}_e}) = (4 \text{ MeV}, 5 \text{ MeV})$ . In the adiabatic range the produced amount of  ${}^7\text{Li}$  through  ${}^4\text{He}(\bar{\nu}_e, e^-n){}^3\text{H}$  does not depend on the initial neutrino temperatures. The different neutrino temperatures lead to different  ${}^7\text{Li}$  yields through  ${}^4\text{He}(\nu, \nu'p){}^3\text{H}$ , which makes virtually larger effect than the neutrino oscillations.

Figure 5c shows the cases of the  ${}^{11}\text{B}$  yield ratios in the case of normal mass hierarchy.

The  $^{11}\text{B}$  yield ratios are 1.31 and 1.23 in the cases of  $(T_{\nu_e}, T_{\bar{\nu}_e})=(3.2 \text{ MeV}, 4 \text{ MeV})$  and  $(4 \text{ MeV}, 5 \text{ MeV})$ , respectively, in adiabatic range. Since most of  $^{11}\text{B}$  is produced by way of  $^7\text{Li}$ , the dependence on the neutrino temperatures is similar to  $^7\text{Li}$ . Some  $^{11}\text{B}$  are produced by way of  $^7\text{Be}$  through  $^7\text{Be}(n, p)^7\text{Li}(\alpha, \gamma)^{11}\text{B}$ . Thus, the difference of  $^{11}\text{B}$  yield due to different neutrino temperatures is smaller in the adiabatic case than in the nonadiabatic case. From the viewpoint of the yield ratios, the  $^{11}\text{B}$  yield ratio is larger in the adiabatic range.

In the case of inverted mass hierarchy (see Fig. 5*d*), the  $^{11}\text{B}$  yield ratios are 1.39 and 1.21 in the cases of  $(T_{\nu_e}, T_{\bar{\nu}_e})=(3.2 \text{ MeV}, 4 \text{ MeV})$  and  $(4 \text{ MeV}, 5 \text{ MeV})$  in the adiabatic range. In the case of  $(T_{\nu_e}, T_{\bar{\nu}_e})=(3.2 \text{ MeV}, 5 \text{ MeV})$  the  $^{11}\text{B}$  yield ratio is 1.35 in the adiabatic range. Thus, the  $^{11}\text{B}$  yield ratios in the cases of  $T_{\nu_e} = 3.2 \text{ MeV}$  are larger than the maximum  $^{11}\text{B}$  yield ratio in normal mass hierarchy. In these cases the  $^7\text{Li}$  yield ratios are correspondingly similar to each other. This reflects the fact that  $^{11}\text{B}$  is mainly produced by way of  $^3\text{H}$  and  $^7\text{Li}$ .

## 5. Discussion

### 5.1. Neutrino Oscillations in Shock Propagating Medium

When we calculated neutrino oscillations, we adopted the density profile of a presupernova and did not consider the shock propagation during supernova explosion. One of the reasons is that our hydrodynamical model assumes the inner boundary of the supernova ejecta as a mass cut and the density structure inside the mass cut is not considered. Indeed, numerical simulations of core collapse, core bounce, and explosion of surrounding materials have not been successful yet (Buras et al. 2003; Sumiyoshi et al. 2005). On the other hand, numerical simulations of the shock propagation from a neutrino sphere to the envelope have been studied using time-dependent inner boundary, i.e., the surface of the neutron star (e.g., Tomàs et al. 2004). In this section we discuss the shock propagation effect on neutrino oscillations using the density profile of the supernova ejecta calculated by hydrodynamical model, and assuming a simple analytical density profile inside the mass cut.

In order to discuss the shock propagation effect on the neutrino oscillations, we take simple analytical density structure inside the mass cut. First, we assume that the density drops as  $\rho \propto r^{-3}$  from a neutrino sphere until it drops to the value at the mass cut. Then, the density stays a constant at the value for the location of the mass cut. The density profile in the present discussion is thus

$$\rho(r) = 1 \times 10^4 \left( \frac{r}{1 \times 10^9 \text{cm}} \right)^{-3} \quad \text{for } r \leq r_c \quad (13)$$

and

$$\rho(r) = \rho_{\text{mcut}} \quad \text{for} \quad r_c \leq r \leq r_{\text{mcut}}, \quad (14)$$

where  $\rho_{\text{mcut}}$  and  $r_{\text{mcut}}$  are the density and radius at the mass cut and  $r_c$  is the radius where the density first drops to  $\rho = \rho_{\text{mcut}}$ . As the shock wave moves outward, the density behind the shock front decreases and the density at the mass cut also drops. Thus,  $r_c$  becomes larger as time passes by.

We now study the influence of the neutrino oscillations with the shock propagation to nucleosynthesis of the light elements. Figure 6 shows the dependence of the  ${}^7\text{Li}$  and  ${}^{11}\text{B}$  yield ratios on  $\sin^2 2\theta_{13}$ . First, we consider the dependence in the normal mass hierarchy. We find in the case of  $\sin^2 2\theta_{13} \gtrsim 1 \times 10^{-4}$  that the yield ratios of both  ${}^7\text{Li}$  and  ${}^{11}\text{B}$  are slightly smaller than the corresponding yield ratios in the presupernova density profile without shock propagation effect. The decrease in the yield ratios is about at most 4% in the case of  $\sin^2 2\theta_{13} \sim 1 \times 10^{-3}$ . The shock propagation effect of the neutrino oscillations is seen in the case of H-resonance close to adiabatic.

Next, we consider the case of inverted mass hierarchy. Compared with the case of normal mass hierarchy, the decrease in the yield ratios are smaller; they are 1% level in the case of  $\sin^2 2\theta_{13} \sim 1 \times 10^{-3}$ . Therefore, we can conclude that in the inverted mass hierarchy not only the effect of neutrino oscillations itself but also the shock propagation effect is smaller than the case of normal mass hierarchy.

The shock propagation effect on the neutrino oscillations is seen in  $5 \sim 10$  s when the shock front reaches the O/C layer or the inner region of the He/C layer. Meantime, the shock wave passes through the H-resonance region. When the shock wave passes through this region, the density becomes higher and the resonance region moves outward in the mass coordinate. At the same time, the density change at the shock front makes the adiabaticity of the resonance slightly smaller. After the shock front has passed the O/C layer, the location of the resonance in the mass coordinate goes inward owing to the density decrease by the expansion. The shock propagation effect is mainly seen in the inner region of the He layer,  $3.8M_{\odot} \lesssim M_r \lesssim 4.3M_{\odot}$ . We have shown in the last section that  ${}^7\text{Be}$  is produced in the region of  $M_r \lesssim 4.8M_{\odot}$  and that  ${}^7\text{Li}$  is produced outside this region. In the normal mass hierarchy the increase in the yield is mainly due to  ${}^7\text{Be}$  production. Therefore, the shock propagation effect is seen more clearly in the normal mass hierarchy.



## 5.2. Dependence on Stellar Models

We investigated the  $\nu$ -process nucleosynthesis with neutrino oscillations using 14E1 model, which is a progenitor model of SN 1987A in Shigeyama & Nomoto (1990). This stellar model corresponds to about  $20 M_{\odot}$  at the zero-age main sequence (ZAMS) and has a He core of  $6.0 M_{\odot}$ . Stars with the mass larger than  $\sim 12 M_{\odot}$  are considered to evolve to form Fe core and become core-collapse supernovae at the end. Their internal structure indicates “onion” shell structure and their abundance distribution depends on their stellar mass at the ZAMS. On the other hand, the treatment of convection also affects the structure of presupernovae. We here discuss the influence of the internal structure to the  $\nu$ -process nucleosynthesis with neutrino oscillations.

Detailed studies of massive star evolution (e.g., Nomoto & Hashimoto 1988; Hashimoto 1995) indicated that the region of the O-rich layers in the presupernova stage increases in larger ZAMS stellar masses. Hashimoto (1995) indicated that 4, 8, and  $16 M_{\odot}$  He star models have the O-rich layers of 0.7, 4.4, and  $11.4 M_{\odot}$  and that the region of the He-rich layers has commonly about masses of  $\sim 2 M_{\odot}$ . Stellar models including semiconvection and convective overshooting mixing also have large O-rich layers (Woosley & Weaver 1988). If the region of the O-rich layers is much larger than that of the He/C layer, most of  $^{11}\text{B}$  would be produced through the  $\nu$ -process from  $^{12}\text{C}$  in the O-rich layers rather than from  $^4\text{He}$  in the He/C layer. On the other hand, the density in the O/C layer scarcely depends on the stellar mass (e.g., Nomoto & Hashimoto 1988; Hashimoto 1995) and the density is close to the density of H-resonance. We showed that the effect of neutrino oscillations is not seen in the O-rich layers. Thus, we expect that the increase in the  $^{11}\text{B}$  yield due to neutrino oscillations is very small if the region of the O-rich layers is larger than the He/C layer and  $^{11}\text{B}$  is mainly produced from  $^{12}\text{C}$ .

The density profile of the He/C layer also may affect the increase in the  $^7\text{Li}$  yield by neutrino oscillations. This is because  $^7\text{Li}$  is produced as  $^7\text{Be}$  in the inner region of the He/C layer and as  $^7\text{Li}$  outside the region. We expect that stellar models which produce more  $^7\text{Be}$  rather than  $^7\text{Li}$  bring about larger increase in the  $^7\text{Li}$  yield due to neutrino oscillations in adiabatic H-resonance and normal mass hierarchy. In our model, the yield of  $^7\text{Be}$  increases by a factor of 3.1 at the maximum, whereas  $^7\text{Li}$  produced through  $^3\text{H}(\alpha, \gamma)^7\text{Li}$  increases by a factor of 1.2 in the normal mass hierarchy. When we consider adiabatic H-resonance and normal mass hierarchy, stellar models that produce  $^7\text{Li}$  as  $^7\text{Be}$  rather than  $^7\text{Li}$  lead to the  $^7\text{Li}$  yield more than twice as that without oscillations. On the other hand, if the contribution from  $^7\text{Li}$  through  $^3\text{H}(\alpha, \gamma)^7\text{Li}$  is large, the increase in the  $^7\text{Li}$  yield due to the oscillation would be smaller in the normal mass hierarchy, and it would be larger in the inverted mass hierarchy. In the latter case, the  $^7\text{Li}$  yield produced through  $^3\text{H}(\alpha, \gamma)^7\text{Li}$  increases by a factor

of 1.5 at the maximum.

The shock propagation effect on the neutrino oscillations would depend on the stellar mass. Less massive stars have smaller O-rich region, so that it takes shorter time until the shock wave arrive at the H-resonance density region. After the shock arrival, the transition probabilities to the other flavors become small and the increase in the rates of charged-current  $\nu$ -process reactions also reduces. Thus, the increase in the  ${}^7\text{Li}$  and  ${}^{11}\text{B}$  yields is expected to be small for supernovae evolved from less massive stars.

### 5.3. $CP$ Phase Effect

In this study, we assume that the  $CP$  phase  $\delta$  is equal to zero because the definite value of  $\delta$  has not been determined from neutrino experiments. Let us briefly discuss the influence of  $CP$  phase on the  ${}^7\text{Li}$  and  ${}^{11}\text{B}$  yields produced through the  $\nu$ -process. We consider the transition probabilities to  $\nu_e$  or  $\bar{\nu}_e$ . Yokomakura et al. (2002) showed exact relations of neutrino transition probabilities in arbitrary matter profile. They showed that the transition probability of  $\nu_e \rightarrow \nu_e$  ( $\bar{\nu}_e \rightarrow \bar{\nu}_e$ ) does not depend on the  $CP$  phase  $\delta$ . From their study, we also obtained that the sum of the transition probabilities of  $\nu_\mu \rightarrow \nu_e$  and  $\nu_\tau \rightarrow \nu_e$  ( $\bar{\nu}_\mu \rightarrow \bar{\nu}_e$  and  $\bar{\nu}_\tau \rightarrow \bar{\nu}_e$ ) does not depend on the  $CP$  phase. Here, we note that  $\nu_\mu$  and  $\nu_\tau$  ( $\bar{\nu}_\mu$  and  $\bar{\nu}_\tau$ ) emitted from a proto-neutron star have a same energy spectrum, i.e., the numbers of  $\nu_\mu$  and  $\nu_\tau$  ( $\bar{\nu}_\mu$  and  $\bar{\nu}_\tau$ ) are same for a given neutrino energy. Since the numbers of  $\nu_\mu$  and  $\nu_\tau$  ( $\bar{\nu}_\mu$  and  $\bar{\nu}_\tau$ ) for a given neutrino energy are same, the transition probability from  $\nu_\mu$  or  $\nu_\tau$  ( $\bar{\nu}_\mu$  or  $\bar{\nu}_\tau$ ) to  $\nu_e$  ( $\bar{\nu}_e$ ) for a given neutrino energy does not depend on the  $CP$  phase, and therefore, the change of the energy spectrum of  $\nu_e$  ( $\bar{\nu}_e$ ) does not depend on the  $CP$  phase, too. We do not expect any influences of the  $CP$  phase to the  ${}^7\text{Li}$  and  ${}^{11}\text{B}$  yields.

### 5.4. Active-sterile neutrinos

It is noted that the existence of the fourth sterile neutrinos may change the effect of supernova light element synthesis on neutrino oscillations. Fetter et al. (2003) considered additional sterile neutrinos with the mass squared difference of  $1 \sim 100 \text{ eV}^2$  from electron neutrinos and investigated the effect of active-sterile neutrino conversion on  $r$ -process in neutrino-driven wind model. The Los Alamos liquid scintillator neutrino detector (LSND) experiment suggested that neutrino oscillations occur with mass squared difference in the range of  $\Delta m^2 = 0.2 \sim 10 \text{ eV}^2$  (Aguilar et al. 2001). They argued that it is difficult to generate neutrons enough to activate the  $r$ -process. Then, they showed that active-sterile

neutrino conversion makes the winds favorable for the  $r$ -process even in the initial condition unfavorable to the  $r$ -process. This is because the active-sterile neutrino conversion ceases  $\nu_e$  and, thus, the neutron depletion by  $n(\nu_e, e^-)p$  is suppressed.

If the active-sterile neutrino conversion occurs effectively just after the onset of supernova explosion, then this conversion may reduce the number of  $\nu_e$  and, therefore, it may reduce  ${}^7\text{Li}$  and  ${}^{11}\text{B}$  yields. It is expected that the active-sterile neutrino conversion occurs in inner region of the O-rich layer or even deeper region ( $\rho \sim 6 \times 10^5 \text{ g cm}^{-3}$  for  $\Delta m^2 = 1 \text{ eV}^2$  and  $\varepsilon_\nu = 20 \text{ MeV}$ ; see Eq. (10)). The decrease in the number of  $\nu_e$  may reduce not only the yields of  ${}^7\text{Li}$  and  ${}^{11}\text{B}$  but also those of heavy neutron-deficient nuclei like  ${}^{138}\text{La}$  and  ${}^{180}\text{Ta}$  more effectively, which are produced through  $(\nu_e, e^-)$  reactions. In practice, the effect of the active-sterile neutrino conversion is still complicated because mixing angles of active-sterile neutrinos have not been determined and the conversion may strongly depend on the mixing angles.

### 5.5. Prospects for Constraining Mass Hierarchy and $\theta_{13}$

We obtained that the  ${}^7\text{Li}$  yield is larger by about a factor of two by taking account of neutrino oscillations of normal mass hierarchy and adiabatic H-resonance compared with that without neutrino oscillations. If we can detect the  ${}^7\text{Li}$  abundance or the abundance ratio of  ${}^7\text{Li}$  to an element that is not affected by the  $\nu$ -process in stars which show clear traces of supernovae and if one compares them with the evaluated abundance or abundance ratio in supernova ejecta as we discussed, we may be able to constrain mass hierarchy and the mixing angle  $\theta_{13}$ . We show the dependence of the number ratio of  ${}^7\text{Li}/{}^{11}\text{B}$  on  $\sin^2 2\theta_{13}$  in Fig. 7. The  ${}^7\text{Li}/{}^{11}\text{B}$  ratio should be better than the abundance of  ${}^7\text{Li}$  itself for observations because the  ${}^7\text{Li}/{}^{11}\text{B}$  ratio is rather insensitive to the uncertainties of supernova neutrinos (Yoshida et al. 2006). When we evaluated the number ratio of  ${}^7\text{Li}/{}^{11}\text{B}$ , we considered the four sets of the temperatures of  $\nu_e$  and  $\bar{\nu}_e$  discussed in §4.3. For all three ranges of normal and inverted mass hierarchies and without neutrino oscillations, the largest and smallest values correspond to the cases of  $(T_{\nu_e}, T_{\bar{\nu}_e}) = (3.2 \text{ MeV}, 4.0 \text{ MeV})$  and  $(4.0 \text{ MeV}, 5.0 \text{ MeV})$ . The  ${}^7\text{Li}/{}^{11}\text{B}$  ratio with  $(T_{\nu_e}, T_{\bar{\nu}_e}) = (4.0 \text{ MeV}, 4.0 \text{ MeV})$  is larger than the result with the neutrino temperatures in our standard model. In the normal mass hierarchy and  $\sin^2 2\theta_{13} \gtrsim 2 \times 10^{-3}$ , the  ${}^7\text{Li}/{}^{11}\text{B}$  ratio is larger than 0.83. The maximum values of the  ${}^7\text{Li}/{}^{11}\text{B}$  ratio in the inverted mass hierarchy and without neutrino oscillations are 0.71 and 0.63. We note that the range of the  ${}^7\text{Li}/{}^{11}\text{B}$  ratio deduced from the uncertainties of the  $\nu_{\mu,\tau}$  temperatures, which have been investigated in Yoshida et al. (2006), is included in the range obtained in the present study. Therefore, the  ${}^7\text{Li}/{}^{11}\text{B}$  number ratio in the normal mass hierarchy and adiabatic H-resonance is larger than

that without the oscillations. The  ${}^7\text{Li}/{}^{11}\text{B}$  ratio could be a tracer of normal mass hierarchy and relatively larger  $\theta_{13}$ , still satisfying the observational constraint of  $\sin^2 2\theta_{13} \leq 0.1$ , if the number ratio of  ${}^7\text{Li}/{}^{11}\text{B}$  is precisely observed.

Recently, measurements of B isotopic ratio in metal poor stars have been challenged by several groups (e.g., Rebull et al. 1998; Rebull, Primas, & Duncan 2000). Since supernovae provide large amount of  ${}^{11}\text{B}$  with small amount of  ${}^{10}\text{B}$ , the stars having traces of a supernova are expected to indicate  ${}^{11}\text{B}/{}^{10}\text{B}$  ratio larger than that of the solar-system composition. Deficiency of B abundance with normal primordial  ${}^7\text{Li}$  is reported in a metal poor star formed in an epoch when supernova nucleosynthesis dominated in the early Galaxy with quenched contribution from the cosmic ray interactions with interstellar medium (Primas, Duncan, & Thorburn 1998; Primas et al. 1999). The ratio of  ${}^7\text{Li}/{}^{11}\text{B}$  in supernovae might be found also in primitive meteorites.

Primitive meteorites should contain supernova-originating materials and  ${}^7\text{Li}/{}^{11}\text{B}$  ratio might constrain the neutrino oscillation parameters. The solar-system  ${}^7\text{Li}/{}^{11}\text{B}$  ratio is 3.11 (Anders & Grevesse 1989). The  ${}^7\text{Li}/{}^{11}\text{B}$  in the Galactic cosmic rays, which is one of the main production sites of Li and B, is evaluated to be 0.58 (Fields et al. 2000). These two values are out of our  ${}^7\text{Li}/{}^{11}\text{B}$  range evaluated in the supernova  $\nu$ -process. Therefore, supernova-originating material should have  ${}^7\text{Li}/{}^{11}\text{B}$  ratios different from those of the solar-system composition and the Galactic cosmic rays, which is a favorable feature for our detectable  ${}^7\text{Li}/{}^{11}\text{B}$  ratio in the range  $0.6 \lesssim N({}^7\text{Li})/N({}^{11}\text{B}) \lesssim 1.0$ . Recently, presolar grains from supernovae have been found and isotopic ratios of C, N, O, Si, and Ti have been measured (e.g. Amari et al. 1992; Nittler et al. 1996). Measurement of B isotopic ratios in the grains has been attempted (Hoppe et al. 2001). Future isotopic and abundance measurements of Li and B would deduce  ${}^7\text{Li}/{}^{11}\text{B}$  ratio in supernovae.

We have to note, however, that there are many uncertainties to evaluate the  ${}^7\text{Li}/{}^{11}\text{B}$  ratio and the Li yield in supernova ejecta. These values depend on the stellar mass at least theoretically. As discussed in §5.2, treatment of convection may also change stellar structure and abundance distribution. Aspherical explosion may produce different amount of light elements. In our study, the energy dependence of  $\nu$ -process reaction cross sections is very simplified: more precise evaluation of the energy dependence is required (Suzuki et al. 2006). In order to evaluate the enhancement factor due to neutrino oscillations, we need to construct more precise nucleosynthesis model in massive star evolution and supernova explosions. We also need to observe  ${}^7\text{Li}/{}^{11}\text{B}$  ratio and Li abundance in stars having traces of a definite supernova.

We showed the possibility of constraining parameters of neutrino oscillations from the viewpoint of nucleosynthesis. The enhancement of  ${}^7\text{Li}/{}^{11}\text{B}$  ratio and  ${}^7\text{Li}$  abundance would be

seen in the normal mass hierarchy and adiabatic H-resonance. There are different approaches to constrain neutrino oscillation parameters. One is to constrain neutrino masses from cosmological observations. Massive neutrinos produced in the early universe affect Cosmic Microwave Background (CMB) power spectrum and structure formation, i.e., the shape of matter power spectrum (review in Elgarøy & Lahav 2005). Constraining the total mass of mass eigenstates of neutrinos ( $m_{\nu,\text{tot}} = m_1 + m_2 + m_3$ ) from cosmological observations has been carried out. An upper limit of the total neutrino mass,  $m_{\nu,\text{tot}} < 0.42$  eV at 95% C.L., has been deduced by fitting cosmological parameters combined with the analyses of Wilkinson Microwave Anisotropy Probe (WMAP) CMB, galaxy clustering, galaxy bias, and Ly $\alpha$  forest of the Sloan Digital Sky Survey (Seljak et al. 2005). In the near future higher precision cosmological observations would reduce upper limit of the total neutrino mass, from which the squared mass difference and mass hierarchy also would be determined.

Observations of Diffuse Supernova Neutrino Background (DSNB) may constrain parameters of neutrino oscillations, too. Although DSNB has not been detected yet, future improved neutrino detectors may detect DSNB. Yüksel, Ando, & Beacom (2005) proposed a gadolinium-enhanced Super-Kamiokande detector by which average  $\bar{\nu}_e$  energy and the total  $\bar{\nu}_e$  energy per supernova are to be measured after five years run. Further, Ando (2004) discussed that, in the inverted mass hierarchy and adiabatic H-resonance, the average  $\bar{\nu}_e$  energy is very different from the expected one without the neutrino oscillations. Therefore, combined with theoretical evaluation of the average  $\bar{\nu}_e$  and  $\bar{\nu}_{\mu,\tau}$  energies emitted from proto-neutron stars, the effect of the neutrino oscillations will be studied and the neutrino oscillation parameters will be constrained.

We have these three different procedures to constrain neutrino oscillation parameters. First, the investigation of the  $\nu$ -process nucleosynthesis in supernovae would provide a piece of evidence for normal mass hierarchy and adiabatic H-resonance. Second, DSNB measurement with improved neutrino detector would reveal a possible proof of inverted mass hierarchy and adiabatic H-resonance. Third, improved cosmological observations would clarify mass hierarchy. Thus, combining the three investigations with each other, we hope to constrain strictly the neutrino oscillation parameters in the future.

## 6. Conclusions

We studied light element nucleosynthesis through the  $\nu$ -process in supernovae taking account of neutrino oscillations. The parameters of neutrino oscillations were adopted from the evaluations through several neutrino experiments. We used a supernova model corresponding to SN 1987A and investigated the dependence of the  ${}^7\text{Li}$  and  ${}^{11}\text{B}$  yields on the

mixing angle  $\theta_{13}$  and mass hierarchy. The obtained results are summarized as follows:

- Neutrino oscillations affect the yields of  ${}^7\text{Li}$  and  ${}^{11}\text{B}$  synthesized in supernova explosions. Especially, the  ${}^7\text{Li}$  yield increases by a factor of 1.9 in the normal mass hierarchy and adiabatic H-resonance ( $\sin^2 2\theta_{13} \gtrsim 2 \times 10^{-3}$ ) compared with that without neutrino oscillations. The  ${}^{11}\text{B}$  yield increases by a factor of 1.3.
- In the inverted mass hierarchy, the increase in the  ${}^7\text{Li}$  and  ${}^{11}\text{B}$  yields is smaller: the yields of  ${}^7\text{Li}$  and  ${}^{11}\text{B}$  increase by factors of 1.3 and 1.2.
- Neutrino oscillations in supernovae make the reaction rates of charged-current  $\nu$ -process reactions larger. The reaction rates of neutral-current  $\nu$ -process reactions do not change. Thus, the final amounts of the  $\nu$ -process products increase by the neutrino oscillations. In our study, main important  $\nu$ -process reactions for the  ${}^7\text{Li}$  and  ${}^{11}\text{B}$  production are  ${}^4\text{He}(\nu, \nu'p){}^3\text{H}(\alpha, \gamma){}^7\text{Li}$ ,  ${}^4\text{He}(\nu, \nu'n){}^3\text{He}(\alpha, \gamma){}^7\text{Be}$ ,  ${}^{12}\text{C}(\nu, \nu'p){}^{11}\text{B}$ , and  ${}^{12}\text{C}(\nu, \nu'n){}^{11}\text{C}$ . When we consider neutrino oscillations, the following charged-current  $\nu$ -process reactions become also important:  ${}^4\text{He}(\nu_e, e^-p){}^3\text{He}(\alpha, \gamma){}^7\text{Li}$ ,  ${}^4\text{He}(\bar{\nu}_e, e^+n){}^3\text{H}(\alpha, \gamma){}^7\text{Be}$ ,  ${}^{12}\text{C}(\nu_e, e^-p){}^{11}\text{C}$ ,  ${}^{12}\text{C}(\bar{\nu}_e, e^+n){}^{11}\text{B}$ .
- The neutrino temperatures also affect the  ${}^7\text{Li}$  and  ${}^{11}\text{B}$  yields due to neutrino oscillations. Large difference of the temperatures of  $\nu_e$  and  $\nu_{\mu,\tau}$  brings about larger increase in the yields compared with those without neutrino oscillations.
- The shock propagation effect on the neutrino oscillations would slightly reduce the increment of the  ${}^7\text{Li}$  and  ${}^{11}\text{B}$  yields. In our model, most of neutrinos pass through the He/C layer before the shock wave arrives at the O/C layer, i.e., the resonance density region. When the shock wave is in the O-rich layers, the density change by the shock does not influence strongly neutrino oscillations.

We would like to thank Koichi Iwamoto, Ken'ichi Nomoto, and Toshikazu Shigeyama for providing the data for the internal structure of progenitor model 14E1 and for helpful discussions. We are also indebted to Yong-Yeon Keum and Masahiro Takada for their valuable discussions. Numerical computations were in part carried out on general common use computer system at Astronomical Data Analysis Center (ADAC) of National Astronomical Observatory of Japan. This work has been supported in part by the Ministry of Education, Culture, Sports, Science and Technology, Grants-in-Aid for Young Scientist (B) (17740130) and Scientific Research (17540275), for Specially Promoted Research (13002001), and Mitsubishi Foundation. T.Y. has been supported by the 21st Century COE Program ‘‘Exploring

New Science by Bridging Particle-Matter Hierarchy” in Graduate School of Science, Tohoku University.

## REFERENCES

- Aguilar, A., et al. (LSND Collaboration) 2001, *Phys. Rev. D*, 64, 112007
- Ahmed, S. N., et al. (SNO Collaboration) 2004, *Phys. Rev. Lett.*, 92, 181301
- Amari, S., Hoppe, P., Zinner, E., & Lewis, R. S. 1992, *ApJ*, 394, L43
- Anders, E. & Grevesse, N. 1989, *Geochim. Cosmochim. Acta*, 53, 197
- Ando, S. 2004, *ApJ*, 607, 20
- Apollonio, M., et al. 2003, *Eur. Phys. J.*, C27, 331
- Araki, T., et al. (KamLAND Collaboration) 2005, *Phys. Rev. Lett.*, 94, 081801
- Ashie, Y., et al. (Super-Kamiokande Collaboration) 2004, *Phys. Rev. Lett.*, 93, 101801
- Balantekin, A. B., & Yüksel, H. 2005, *New J. Phys.*, 7, 51
- Bionta, R., et al. 1987, *Phys. Rev. Lett.*, 58, 1494
- Buras, R., Rampp, M., Janka, H.-Th., & Kifonidis, K. 2003, *Phys. Rev. Lett.*, 90, 1101
- Colella, P. & Woodward, P. R. 1984, *J. Comput. Phys.*, 54, 174
- Dighe, A. S. & Smirnov, A. Y. 2000, *Phys. Rev. D*, 62, 033007
- Domogatsky, G. V., Eramzhyan, R. A. & Nadyozhin, D. K. 1978, in *Proc. Int. Conf. on Neutrino Physics and Neutrino Astrophysics*, ed. M. A. Markov, G. V. Domogatsky, A. A. Komar, & A. N. Tavkhelidze (Moscow: Nauka), 115
- Elgarøy, Ø & Lahav, O. 2005, *New J. Phys.*, 7, 61
- Fetter, J., McLaughlin, G. C., Balantekin, A. B., & Fuller, G. M. 2003, *Astroparticle Phys.*, 18, 433
- Fields, B. D., Olive, K. A., Vangioni-Flam, E., & Cassé, M. 2000, *ApJ*, 540, 930
- Goriely, S., Arnould, M., Borzov, I., & Rayet, M. 2001, *A&A*, 375, L35

- Hashimoto, M. 1995, *Prog. Theor. Phys.*, 94, 663
- Heger, A., Kolbe, E., Haxton, W. C., Langanke, K., Martínez-Pinedo, G., & Woosley, S. E. 2005, *Phys. Lett. B*, 606, 258
- Hirata, K., Kajita, T., Koshihara, M., Nakahata, M., & Oyama, Y. 1987, *Phys. Rev. Lett.*, 58, 1490
- Hoppe, P., Lodders, K., Strebels, R., Amari, S., & Lewis, R. S. 2001, *ApJ*, 551, 478
- Keil, M. Th., Raffelt, G. G., & Janka, H.-Th. 2003, *ApJ*, 590, 971
- Kimura, K., Takamura, A., & Yokomakura, H. 2002a, *Phys. Lett. B*, 537, 86
- Kimura, K., Takamura, A., & Yokomakura, H. 2002b, *Phys. Rev. D*, 66, 073005
- Lattimer, J. M. & Prakash, M. 2001, *ApJ*, 550, 426
- Lattimer, J. M. & Yahil, A. 1989, *ApJ*, 340, 426
- McKeown, R. D. & Vogel, P. 2004, *Phys. Rep.*, 394, 315
- Nittler, L. R., Amari, S., Zinner, E., Woosley, S. E., & Lewis, R. S. 1996, *ApJ*, 462, L31
- Nomoto, K. & Hashimoto, M. 1988, *Phys. Rep.*, 163, 13
- Otsuki, K., Tagoshi, H., Kajino, T., & Wanajo, S. 2000, *ApJ*, 533, 424
- Rauscher, T., Heger, A., Hoffman, R. D., & Woosley, S. E. 2002, *ApJ*, 576, 323
- Rebull, L., Duncan, D., Johansson, S., Thorburn, J., & Fields, B. 1998, *ApJ*, 507, 387
- Rebull, L., Primas, F., & Duncan, D. 2000, in *The First Stars*, eds. A. Weiss, T. G. Abel, & V. Hill (ESO Astrophysics Symposia; Berlin: Springer), 176
- Primas, F., Duncan, D. K., Peterson, R. C., & Thorburn, J. A. 1999, *A&A*, 343, 545
- Primas, F., Duncan, D. K., & Thorburn, J. A. 1998, *ApJ*, 506, L51
- Seljak, U., et al. 2005, *Phys. Rev. D*, 71, 103515
- Shigeyama, T. & Nomoto, K. 1990, *ApJ*, 360, 242
- Shigeyama, T., Nomoto, K., Yamaoka, H., & Thielemann, F.-K. 1992, *ApJ*, 386, L13
- Sumiyoshi, K., Suzuki, H., Yamada, S., & Toki, H. 2004, *Nucl. Phys. A*, 730, 227



- Suzuki, T., Chiba, S., Yoshida, T., Kajino, T. & Otsuka, T. 2006, Phys. Rev. C, to be submitted.
- Takahashi, K. & Sato, K. 2003, Prog. Theor. Phys., 109, 919
- Takahashi, K., Sato, K., Dalhed, H. E., & Wilson, J. R. 2003, Astroparticle Phys., 20, 189
- Takahashi, K., Watanabe, M., Sato, K., & Totani, T. 2001, Phys. Rev. D, 64, 093004
- Takahashi, K., Wittl, J., & Janka, H.-Th. 1994, A&A, 286, 857
- Terasawa, M., Langanke, K., Mathews, G. J., Kajino, T., & Kolbe, E. 2004, ApJ, 608, 470
- Tomàs, R., Kachelrieß, M., Raffelt, G., Dighe, A., Janka, H.-T., & Scheck, L. 2004, J. Cosmology and Astroparticle Phys., 9, 15
- Woosley, S. E., Hartmann, D. H., Hoffman, R. D., & Haxton, W. C. 1990, ApJ, 356, 272
- Woosley, S. E. & Weaver, T. A. 1988, Phys. Rep., 163, 79
- Woosley, S. E. & Weaver, T. A. 1995, ApJS, 101, 181
- Woosley, S. E., Wilson, J. R., Mathews, G. J., Hoffman, R. D., & Meyer, B. S. 1994, ApJ, 433, 229
- Yüksel, H., Ando, S., & Beacom, J. F. 2005, astro-ph/0509297
- Yokomakura, H., Kimura, K., & Takamura, A. 2002, Phys. Lett., B544, 286
- Yoshida, T., Emori, H. & Nakazawa, K. 2000, Earth Planets Space, 52, 203
- Yoshida, T., Kajino, T., & Hartmann, D. H. 2005, Phys. Rev. Lett., 94, 231101
- Yoshida, T., Kajino, T., Yokomakura, H., Kimura, K., Takamura, A. & Hartmann, D. H. 2006, Phys. Rev. Lett., 96, 091101
- Yoshida, T., Terasawa, M., Kajino, T., & Sumiyoshi, K. 2004, ApJ, 600, 204

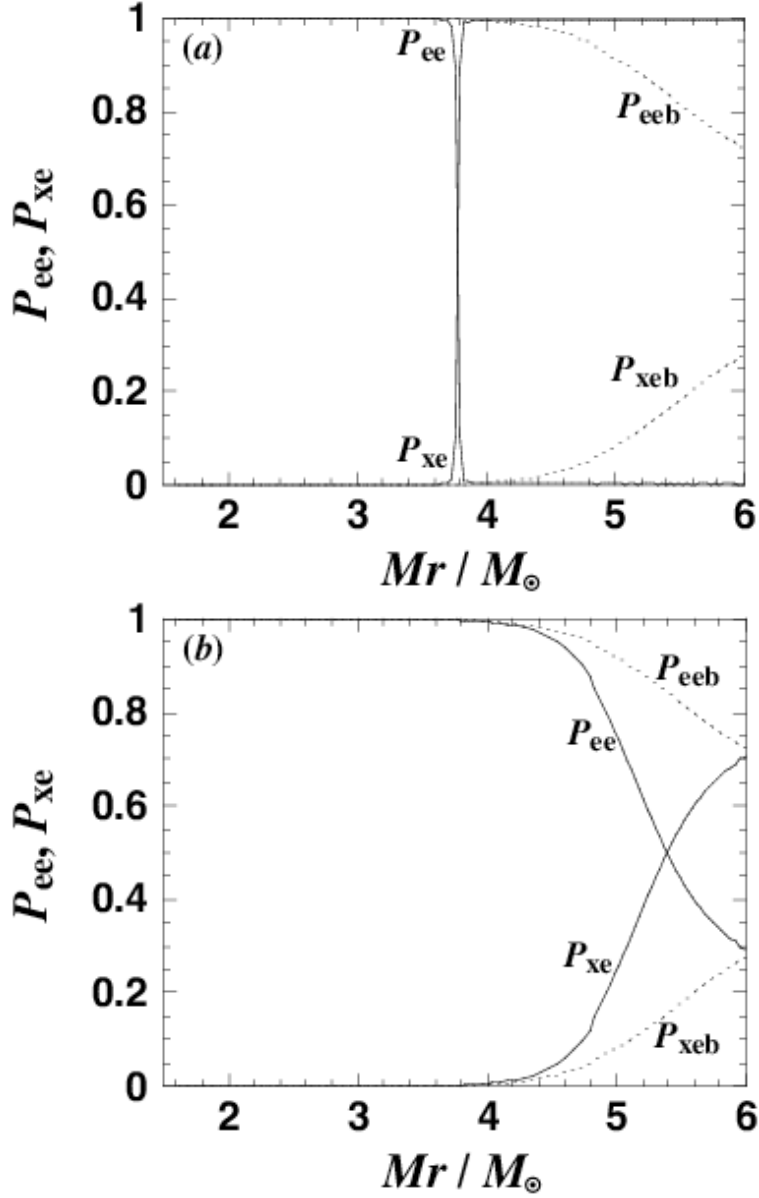


Fig. 1.— Transition probabilities by neutrino oscillations in the normal mass hierarchy. The value of  $\sin^2 2\theta_{13}$  is (a)  $1 \times 10^{-2}$  and (b)  $1 \times 10^{-6}$ . Solid lines are the transition probabilities from  $\nu_e$  to  $\nu_e$ ,  $P_{ee}$ , and from  $\nu_{\mu,\tau}$  to  $\nu_e$ ,  $P_{xe}$ . Dashed lines are those from  $\bar{\nu}_e$  to  $\bar{\nu}_e$ ,  $P_{eeb}$ , and from  $\bar{\nu}_{\mu,\tau}$  to  $\bar{\nu}_e$ ,  $P_{xeb}$ . Horizontal axis is the mass coordinates in units of  $M_\odot$ . The neutrino energy is set to be 50 MeV.

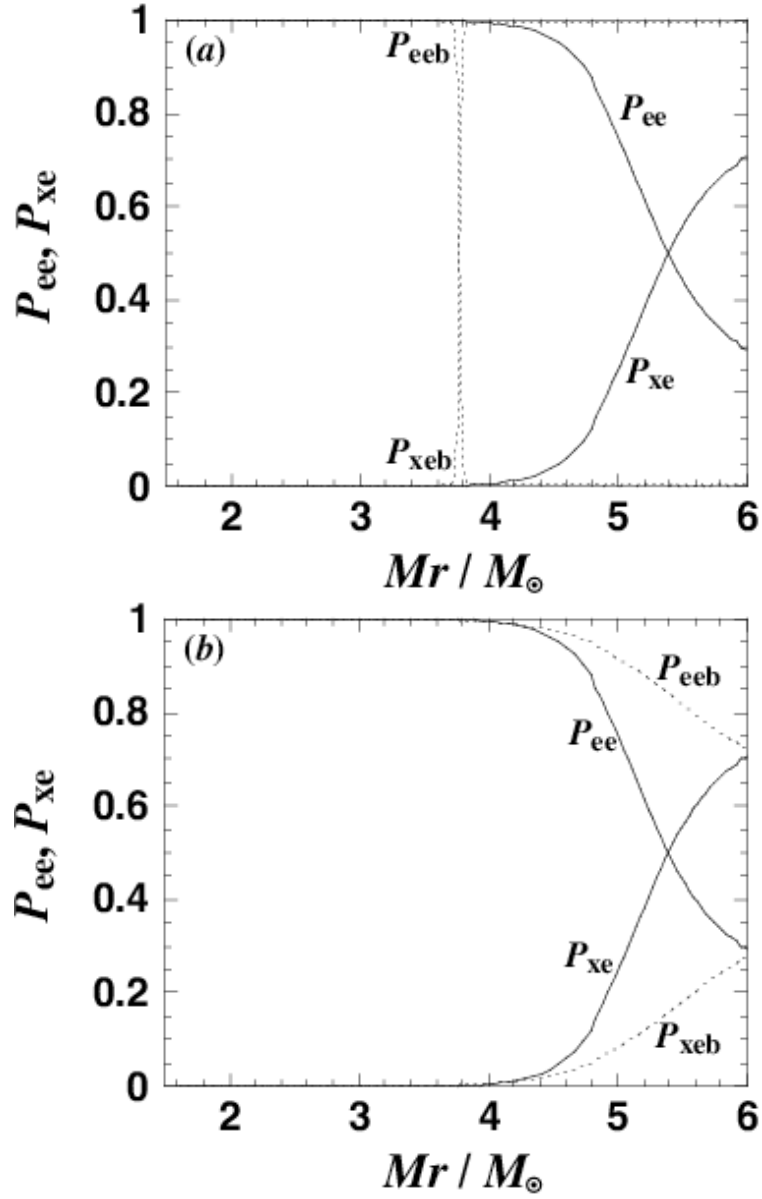


Fig. 2.— The same as Fig. 1 but for the inverted mass hierarchy.

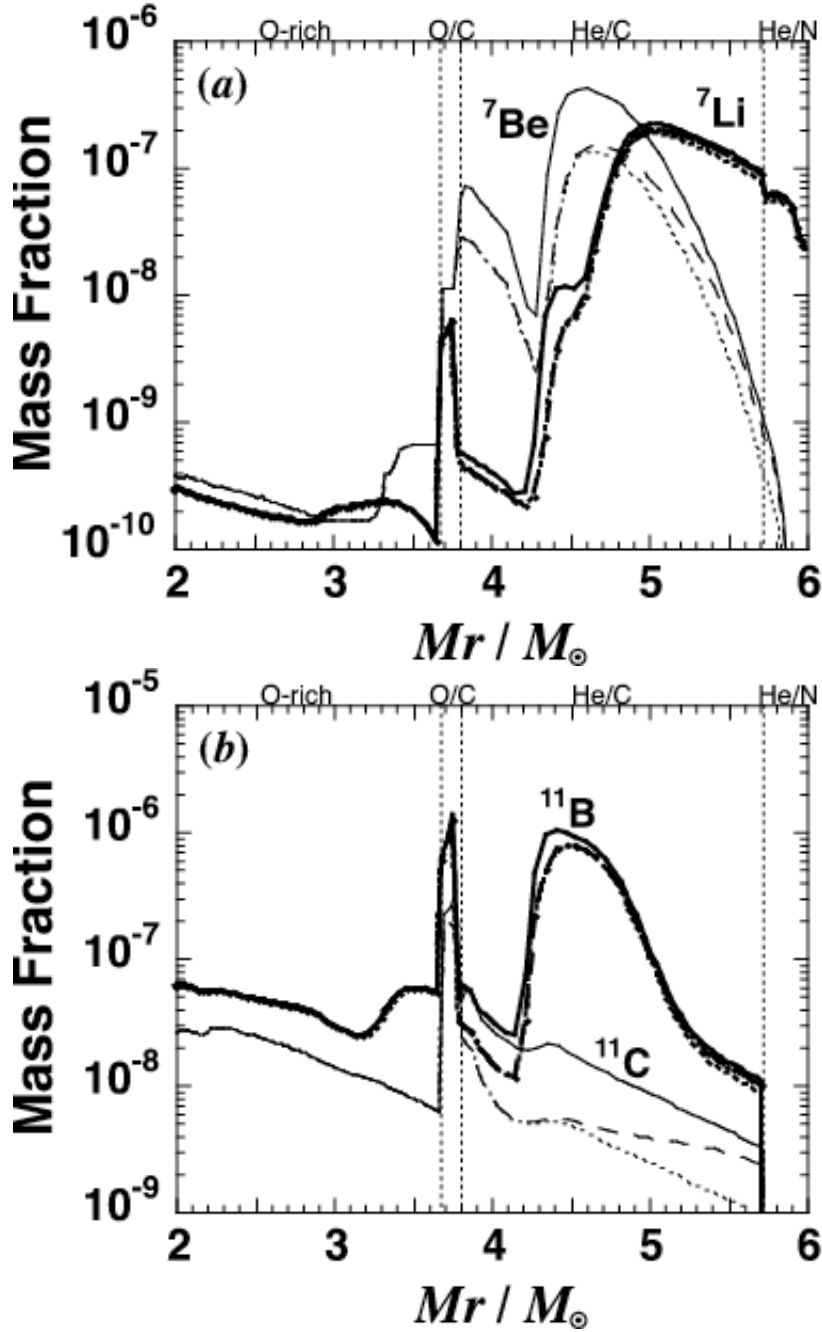


Fig. 3.— Mass fraction distribution of  ${}^7\text{Li}$  and  ${}^{11}\text{B}$  in the normal mass hierarchy ((a) and (b)) and inverted mass hierarchy ((c) and (d)) as a function of the mass coordinate in units of  $M_\odot$ . O-rich, O/C, He/C, and He/N indicate the O-rich, O/C, He/C, and He/N layers in the supernova ejecta. Thick lines and thin lines correspond to the mass fractions of  ${}^7\text{Li}$  and its isobar  ${}^7\text{Be}$ , respectively, in (a) and (c), and those of  ${}^{11}\text{B}$  and its isobar  ${}^{11}\text{C}$ , respectively, in (b) and (d). Solid lines and dashed lines correspond to the cases of  $\sin^2 2\theta_{13} = 1 \times 10^{-2}$  and  $1 \times 10^{-6}$ . The mass fractions calculated without neutrino oscillations are indicated by dotted lines.

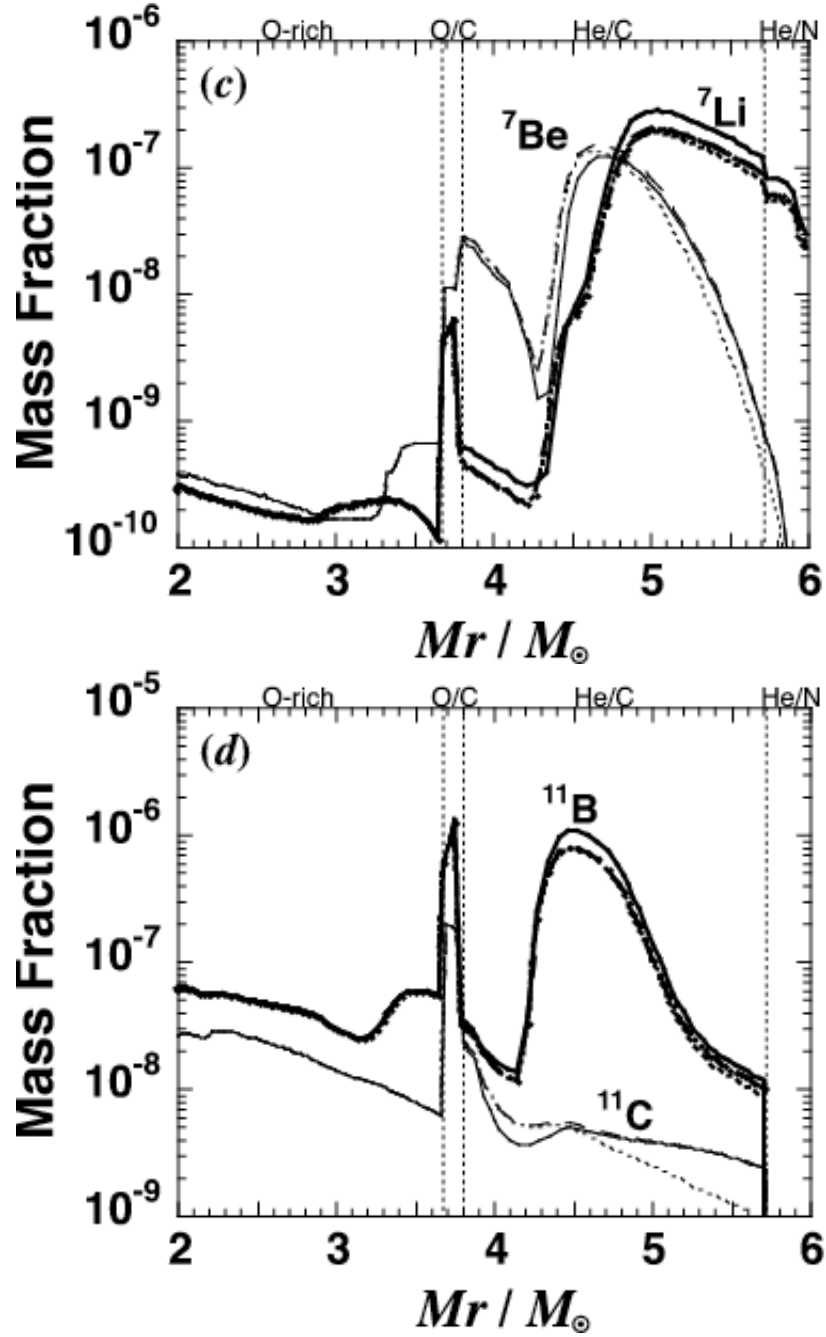


Fig. 3.— *Continued.*

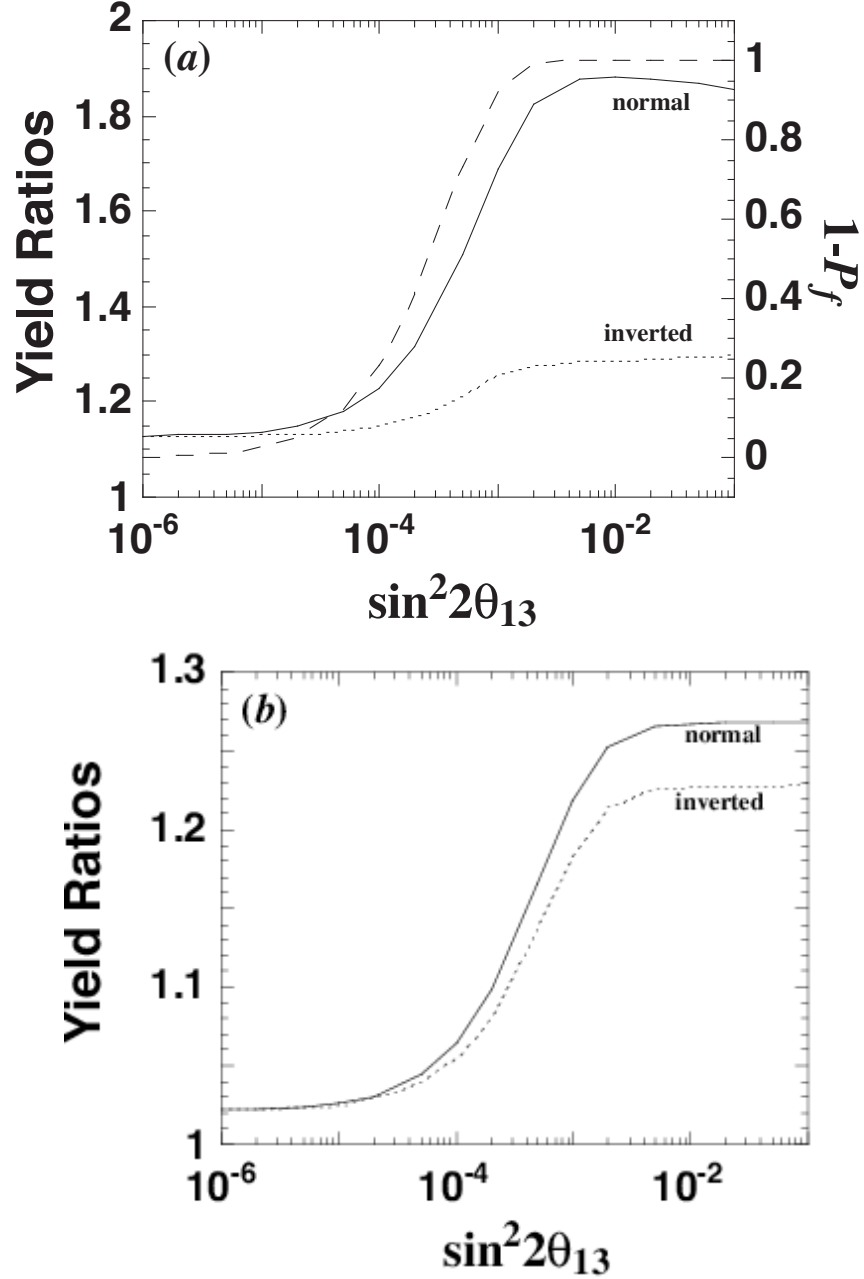


Fig. 4.— Dependence of the yield ratios of (a)  ${}^7\text{Li}$  and (b)  ${}^{11}\text{B}$  on  $\sin^2 2\theta_{13}$ . Solid line and dotted line indicate the yield ratios in the normal and inverted mass hierarchies. In panel (a), dashed line indicates the flip probability in the case of neutrino energy equal to 50 MeV as the formulation of  $1 - P_f$ .

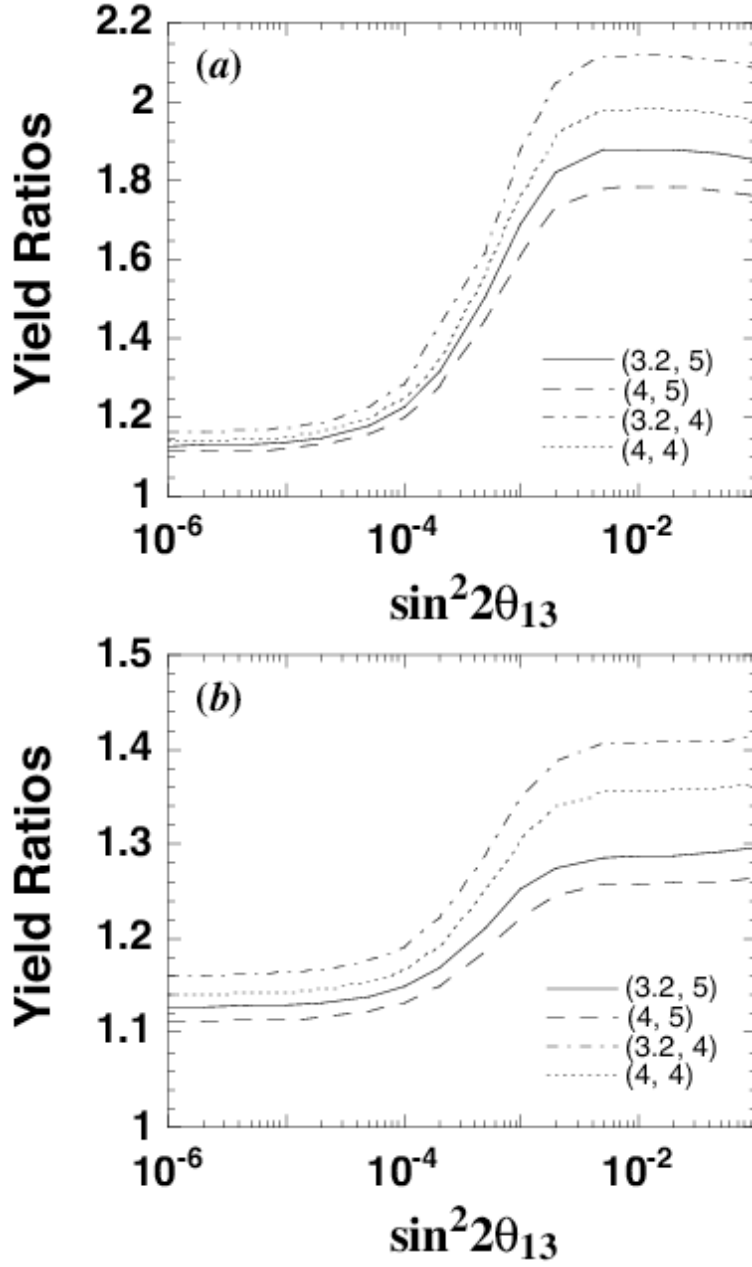


Fig. 5.— Yield ratios of  ${}^7\text{Li}$  ((a) and (b)) and  ${}^{11}\text{B}$  ((c) and (d)) related to the temperatures of  $\nu_e$  and  $\bar{\nu}_e$  emitted from a proton-neutron star. Panels (a) and (c) correspond to the normal mass hierarchy and panels (b) and (d) correspond to the inverted mass hierarchy. Solid, dashed, dash-dotted, and dotted lines indicate the yield ratios in the cases of  $(T_{\nu_e}, T_{\bar{\nu}_e}) = (3.2 \text{ MeV}, 5 \text{ MeV}), (4 \text{ MeV}, 5 \text{ MeV}), (3.2 \text{ MeV}, 4 \text{ MeV}),$  and  $(4 \text{ MeV}, 4 \text{ MeV})$ .

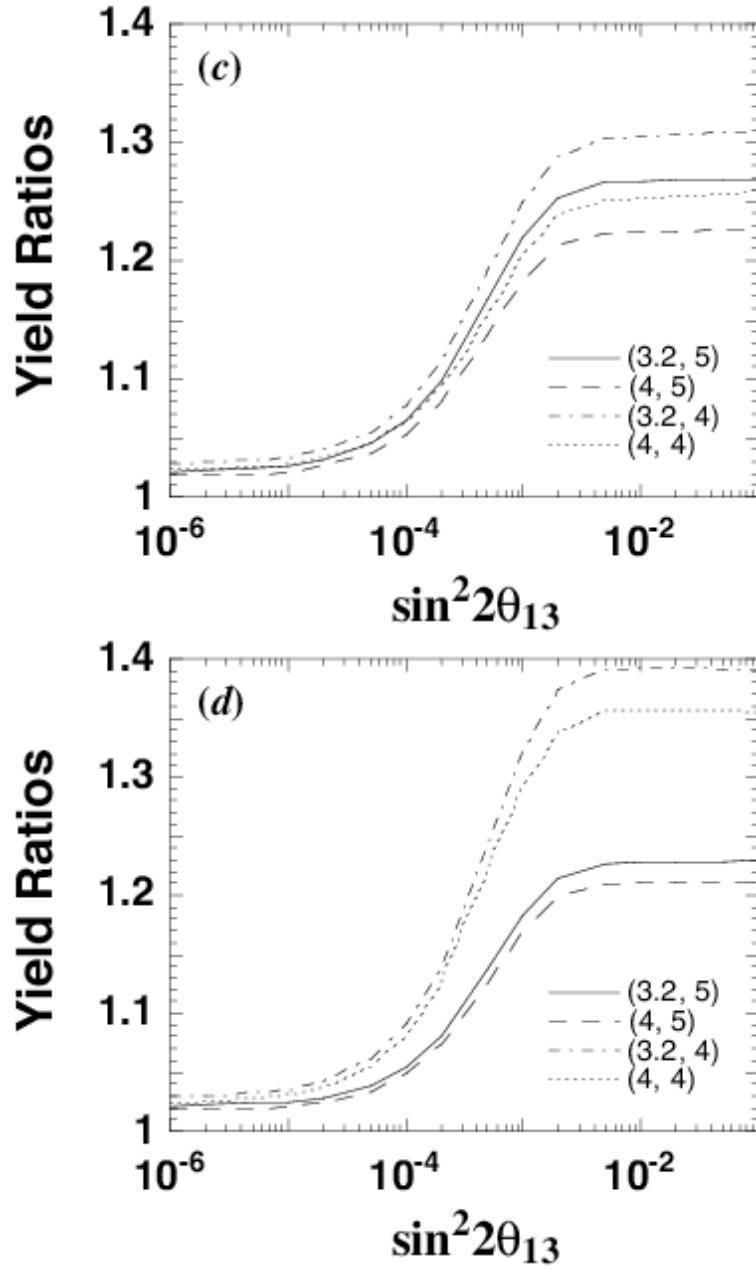


Fig. 5.— *Continued.*



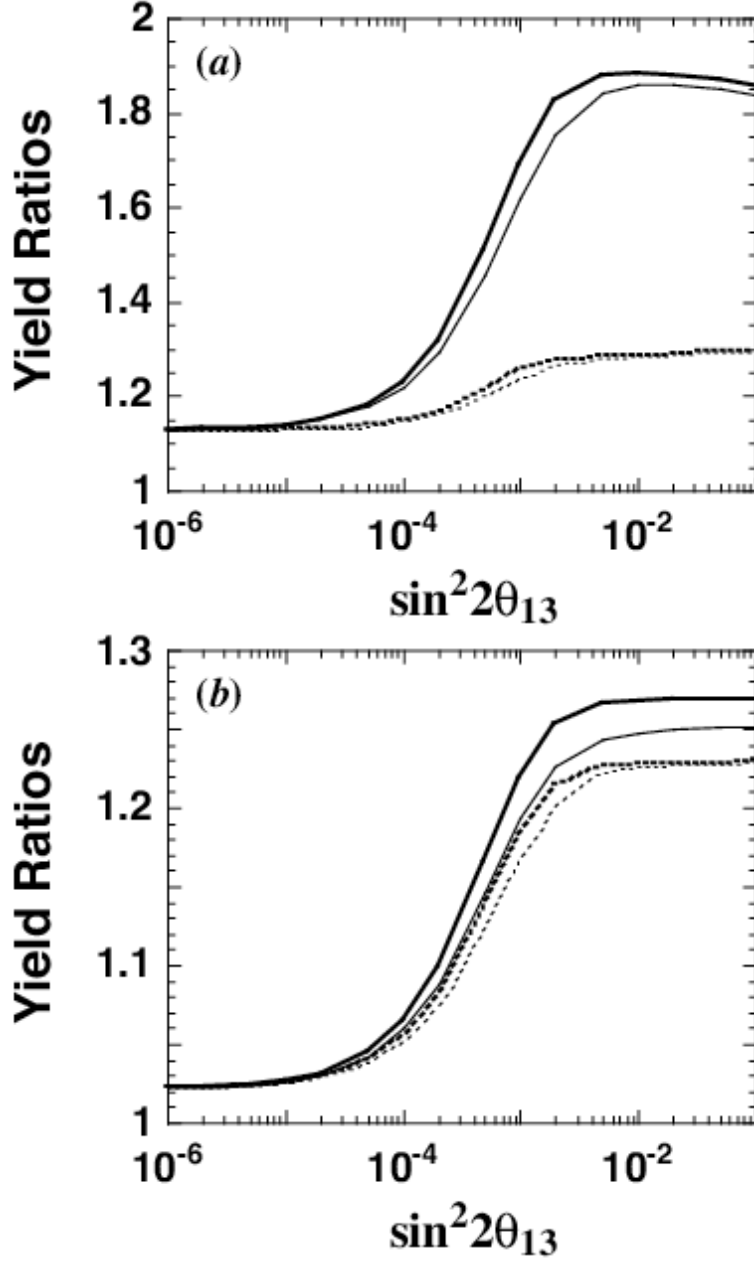


Fig. 6.— Dependence of the (a)  ${}^7\text{Li}$  and (b)  ${}^{11}\text{B}$  yield ratios on  $\sin^2 2\theta_{13}$  taking account of the shock propagation effect on neutrino oscillations. Solid lines and dotted lines correspond to the normal and inverted mass hierarchies. Thick lines are the same as in Fig. 4. Thin lines indicate the yield ratios taking into account the shock propagation effect.

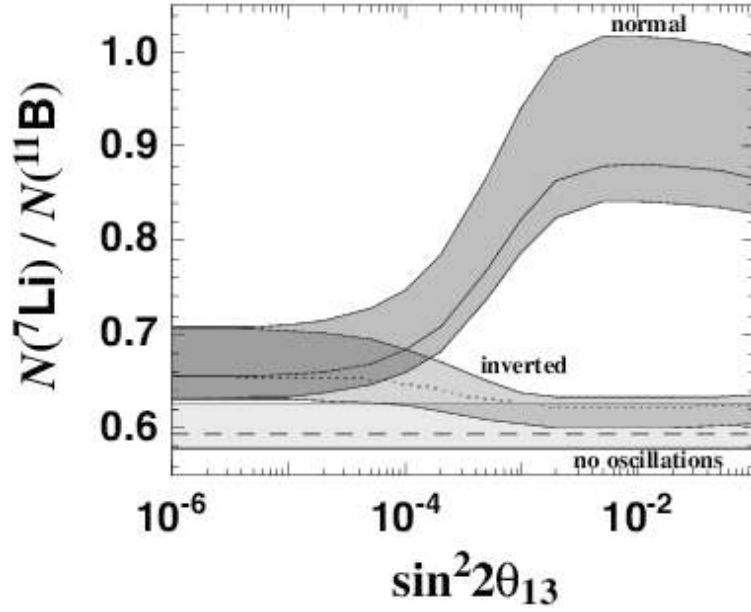


Fig. 7.— Dependence of the  $^7\text{Li}/^{11}\text{B}$  number ratio on  $\sin^2 2\theta_{13}$ . The dark- and medium-shaded regions indicate the ranges of the  $^7\text{Li}/^{11}\text{B}$  ratios in the normal and inverted mass hierarchies. The number ratio without the neutrino oscillations is indicated by the light-shaded region. These regions are obtained from the evaluations using four sets of the temperatures of  $\nu_e$  and  $\bar{\nu}_e$  defined in §4.3. Solid, dotted, and dashed lines in each region correspond to the number ratio with our standard model of the neutrino temperatures (see §4.3). See text for more details.

Table 1: Coefficients and threshold energies of the cross sections for charged-current reactions on  ${}^4\text{He}$  and  ${}^{12}\text{C}$ . The evaluated cross sections are in units of  $10^{-42} \text{ cm}^2$ .

| Reaction  | $a$                      | $b$     | $\varepsilon_{th}$ (MeV) |
|---|--------------------------|---------|--------------------------|
| ${}^4\text{He}(\nu_e, e^-p){}^3\text{He}$                 | $2.45027 \times 10^{-6}$ | 4.03496 | 19.795                   |
| ${}^4\text{He}(\bar{\nu}_e, e^+n){}^3\text{H}$            | $2.37357 \times 10^{-5}$ | 3.31394 | 21.618                   |
| ${}^{12}\text{C}(\nu_e, e^-p){}^{11}\text{C}$             | $3.73589 \times 10^{-6}$ | 3.78171 | 17.939                   |
| ${}^{12}\text{C}(\bar{\nu}_e, e^+n){}^{11}\text{B}$       | $2.76414 \times 10^{-5}$ | 3.08738 | 17.761                   |
| ${}^{12}\text{C}(\nu_e, e^- \gamma){}^{12}\text{N}$       | $2.45749 \times 10^{-3}$ | 1.88899 | 17.3381                  |
| ${}^{12}\text{C}(\bar{\nu}_e, e^+ \gamma){}^{12}\text{B}$ | $2.13890 \times 10^{-3}$ | 1.72299 | 14.3909                  |

Table 2: Yields of  ${}^7\text{Li}$  and  ${}^{11}\text{B}$  without neutrino oscillations for four sets of the adopted temperatures of  $\nu_e$  and  $\bar{\nu}_e$ . The temperature of  $\nu_{\mu,\tau}$  and  $\bar{\nu}_{\mu,\tau}$  is assumed commonly to be 6.0 MeV (see §2.2).

| $(T_{\nu_e}, T_{\bar{\nu}_e})$ | $M({}^7\text{Li})/M_\odot$ | $M({}^{11}\text{B})/M_\odot$ |
|--------------------------------|----------------------------|------------------------------|
| (3.2 MeV, 5 MeV)               | $2.36 \times 10^{-6}$      | $6.26 \times 10^{-6}$        |
| (4 MeV, 4 MeV)                 | $2.24 \times 10^{-6}$      | $5.77 \times 10^{-6}$        |
| (4 MeV, 5 MeV)                 | $2.50 \times 10^{-6}$      | $6.80 \times 10^{-6}$        |
| (3.2 MeV, 4 MeV)               | $2.08 \times 10^{-6}$      | $5.23 \times 10^{-6}$        |